

Direct Analysis of Spectra of the Peculiar Type Ia Supernova 2000cx

David Branch¹, R. C. Thomas^{1,2}, E. Baron¹, Daniel Kasen², Kazuhito Hatano³,
K. Nomoto³, Alexei V. Filippenko⁴, Weidong Li⁴, and Richard. J. Rudy⁵

ABSTRACT

The Type Ia SN 2000cx exhibited multiple peculiarities, including a lopsided B -band light-curve peak that does not conform to current methods for using shapes of light curves to standardize SN Ia luminosities. We use the parameterized supernova synthetic-spectrum code **Synow** to study line identifications in the photospheric-phase spectra of SN 2000cx. Previous work established the presence of Ca II infrared-triplet features forming above velocity $\sim 20,000$ km s⁻¹, much higher than the photospheric velocity of $\sim 10,000$ km s⁻¹. We find Ti II features forming at the same high velocity. High-velocity line formation is partly responsible for the photometric peculiarities of SN 2000cx: for example, B -band flux blocking by Ti II absorption features that decreases with time causes the B light curve to rise more rapidly and decline more slowly than it otherwise would.

SN 2000cx contains an absorption feature near 4530 Å that may be H β , forming at the same high velocity. The lack of conspicuous H α and P α signatures does not necessarily invalidate the H β identification if the high-velocity line formation is confined to a clump that partly covers the photosphere and the H α and P α source functions are elevated relative to that of resonance scattering. The H β identification is tentative. If it is correct, the high-velocity matter must have come from a nondegenerate companion star.

Subject headings: supernovae: general – supernovae: individual (SN 2000cx)

¹Department of Physics and Astronomy, University of Oklahoma, Norman, Oklahoma 73019, USA; branch@nhn.ou.edu

²Lawrence Berkeley National Laboratory, 1 Cyclotron Road, Berkeley, CA 94720–8158

³Department of Astronomy and Research Center for the Early Universe, University of Tokyo, Bunkyo-ku, Tokyo, Japan

⁴Department of Astronomy, 601 Campbell Hall, University of California, Berkeley, CA 94720–3411

⁵Space Science Applications Laboratory, The Aerospace Corporation M2/266, P. O. Box 92957, Los Angeles, CA 90009

1. INTRODUCTION

Supernova 2000cx in NGC 524 was an intriguing Type Ia (SN Ia) event. [See Filippenko (1997) for an overview of supernovae.] Li et al. (2001; hereafter L01) presented extensive optical photometric and spectroscopic observations that revealed multiple peculiarities, including the following: (1) Around the time of maximum brightness the B -band light curve rose rapidly but declined slowly, resulting in a lopsided light-curve shape that does not conform to present SN Ia light-curve fitting techniques such as the multicolor light-curve-shape (MLCS) method of Riess, Press, & Kirshner (1996) or the stretch method of Perlmutter et al. (1997) and Goldhaber et al. (2001). (2) Around maximum brightness the $B - V$ color was redder than that of a normal SN Ia, but after about 15 days postmaximum $B - V$ was bluer than normal. (3) In certain respects (strong Fe III, weak Si II and S II) the premaximum spectra resembled those of the peculiar overluminous SN 1991T (Filippenko et al. 1992a), but the postmaximum spectral evolution differed from that of both SN 1991T and normal SNe Ia. Fe III lines persisted for an unusually long time after maximum brightness while Fe II lines were late to make their appearance. L01 discussed the implications of their observations for the physical nature of SN 2000cx and tentatively suggested that it may have been an overluminous event with an even larger yield of ^{56}Ni and a higher ejecta kinetic energy than SN 1991T.

Rudy et al. (2002; hereafter R02) obtained infrared spectra of SN 2000cx, 5 and 6 days before maximum brightness, covering the range 0.8 to 2.5 μm . Following Meikle et al. (1996) and Wheeler et al. (1998), who attributed an absorption near 1.05 μm in the normal SN Ia 1994D to Mg II $\lambda 10296$, R02 identified a 1.02 μm absorption in SN 2000cx with the same transition, but forming at unusually high velocity. They inferred that freshly synthesized magnesium extended to velocities higher than 20,000 km s^{-1} , and discussed this finding as support for a delayed detonation explosion model, rather than a deflagration model, for SN 2000cx.

Candia et al. (2003; hereafter C03) presented additional optical and infrared photometry and emphasized that SN 2000cx displayed some characteristics of an *underluminous* SN Ia, including a rather fast bolometric light curve. With a recession velocity of only ~ 2200 km s^{-1} , NGC 524 is not in the Hubble flow, and various ways of estimating its distance span a wide range, so C03 were not able to decide whether SN 2000cx actually was overluminous or underluminous.

In Thomas et al. (2003; hereafter T03) we concentrated on exploring simple explanations for high-velocity ($\sim 22,000$ km s^{-1}) absorption features produced by the Ca II infrared triplet. Our favored solution was a high-velocity non-spherical structure (hereafter a “clump”) that only partly covered the photosphere. We also noted that $\text{H}\beta$ might be

present in absorption at the same high velocity.

Some of the line identifications in the articles cited above were tentative, and many of the spectral features were not identified at all. Here we use the parameterized supernova synthetic-spectrum code **Synow** to study line identifications in the photospheric-phase spectra of SN 2000cx. We also try to shed some light on the causes of the peculiar B light curve and $B - V$ color curve.

2. AN OVERVIEW OF THE SPECTRA AND THE ANALYSIS

The spectra we have studied are shown in Figure 1. The optical spectra, from L01, range from their earliest spectrum, obtained 3 days before the time of maximum brightness in the B band, to 32 days after maximum, when the spectrum was beginning to make the transition from the photospheric to the nebular phase. The infrared spectrum is the sum of the two spectra obtained by R02, 5 and 6 days before maximum; hereafter we will refer to this as the day -5.5 spectrum. A few of the familiar SN Ia absorption features in the optical, produced by Si II, S II, and Ca II, are labelled. In Figure 1 the logarithm of the wavelength is plotted, to allow a fair comparison of the widths of the spectral features at different wavelengths. In subsequent figures the more traditional practice of plotting wavelength is followed. As Figure 1 shows, the spectra did not change very much between days -3 and 7, although there are some significant differences that we will examine below. The changes between days 7 and 15, and especially between days 15 and 32, are much more obvious.

In a recent article (Branch et al. 2003; hereafter B03) we used **Synow** to carry out a direct analysis of early spectra of the normal SN Ia 1998aq. Instead of repeating the discussion of the code and the input parameters, we refer the reader to B03. In §3 we present a detailed discussion of the day 2 spectrum of SN 2000cx. In §4 we more briefly discuss the day 7, 15, and 32 spectra. In §5 we examine the premaximum spectra, beginning with the day -3 spectrum. When analyzing the optical spectra we restrict our attention to wavelengths shorter than 7000 \AA , since the longer wavelength region containing the Ca II infrared triplet was discussed by T03. The day -5.5 infrared spectrum also is considered in §5. The results are discussed in §6.

3. THE DAY 2 SPECTRUM

The day 2 spectrum of SN 2000cx is shown in Figure 2 with its absorption features labelled by wavelength. The same spectrum is compared with a day 2 spectrum of SN 1998aq

in Figure 3. Ions used by B03 to fit the absorption features in SN 1998aq are indicated. By the standards of SNe Ia near maximum light, the differences between these two spectra are large. In SN 2000cx, the absorptions that the two events have in common are more blueshifted, and the prominent Si II and S II absorptions are weaker. SN 2000cx has distinct absorptions at 3900 and 4530 Å that are missing or weaker in SN 1998aq, while SN 1998aq has an absorption at 4420 Å, attributed by B03 to Si III, that is missing or weaker in SN 2000cx. Clearly the main reason that the $B - V$ color of SN 2000cx was redder than that of SN 1998aq at this epoch is that from 3900 to 4300 Å the spectrum of SN 2000cx is strongly depressed compared to that of SN 1998aq. The weaker S II absorptions of SN 2000cx also contribute to making its $B - V$ redder. [It should be mentioned that although SN 1998aq had normal SN Ia spectral features, its $B - V$ color was somewhat bluer than average (Boffi & Riess 2003; A. G. Riess et al., in preparation)].

We used **Synow** to calculate numerous synthetic spectra for comparison with the day 2 spectrum, considering all ions that can be regarded as plausible according to the supernova spectrum atlas of Hatano et al. (1999b). The fitting process was unusually lengthy because it proved necessary to consider line formation at both photospheric velocities (PV, $\sim 10,000$ km s $^{-1}$) and at high velocity (HV, $\sim 20,000$ km s $^{-1}$). Rather than using excitation temperatures as fitting parameters we used the ion-specific default values (see B03) for PV line formation and a nominal value of 5000 K for HV line formation. We began with $v_e = 1000$ km s $^{-1}$ as the default optical-depth e-folding velocity, but (as reported in the tables) in some instances we used larger values of v_e to improve the fits.

Figure 4 shows a comparison of the day 2 spectrum with a synthetic spectrum that has $v_{phot} = 11,000$ km s $^{-1}$, $T_{bb} = 9000$ K, and contains lines of nine ions: Mg II, Si II, S II, Fe III, Co II, and Ni II have only PV components; Ca II has both PV and HV components; Ti II and Fe II have only HV components. The ion-specific input parameters — the wavelength and maximum optical depth of the reference line, the minimum, maximum, and optical-depth e-folding velocities, and the excitation temperature — are listed in Table 1. Except for Ca II the PV ions are mildly detached from the photosphere, at 13,000 km s $^{-1}$. (Detached refers to non-zero line optical depths beginning not at the photospheric velocity but at a higher detachment velocity. By mildly detached we mean that the difference between the two velocities is rather small.) When these ions are undetached at 11,000 km s $^{-1}$ their absorptions are not blueshifted enough. When v_{phot} is increased from 11,000 to 13,000 km s $^{-1}$, so that these ions become undetached at 13,000 km s $^{-1}$, the red edge of the Ca II H&K absorption is too blueshifted and most of the features are slightly too broad. It is not clear, however, that the small difference between the adopted photospheric velocity of 11,000 km s $^{-1}$ and a detachment velocity of 13,000 km s $^{-1}$ is physically significant; it may simply reflect the limitations of **Synow** (e.g., the sharp photosphere assumption).

The overall fit in Figure 4 is fairly good, but there are several obvious discrepancies. As usual with SNe Ia, the observed spectrum is more strongly peaked in the middle of the optical spectrum than a blackbody spectrum. We use a blackbody continuum temperature T_{bb} that works well for the middle of the spectrum because that is where the most interesting line identification issues (HV Ti II, $H\beta$; see below) turn out to be. Therefore the red end of the synthetic spectrum, beginning near 5300 Å, is too high. Obtaining a good fit to the shape of the overall energy distribution is a task for more detailed spectrum calculations, such as those of Lentz et al. (2001). The synthetic spectrum has a peak at 3950 Å that is too high, and it does not fit well at wavelengths shorter than 3600 Å; the fit could be improved by introducing more iron-peak ions, but with more adjustable parameters. The most interesting discrepancy is the lack of a synthetic counterpart to the 4530 Å absorption. We will return to this below.

Figure 5 is like Figure 4 but with only the PV components in the synthetic spectrum. The long-wavelength half of the synthetic spectrum is dominated by PV features of Si II, S II, and Fe III, but at shorter wavelengths the PV-only fit is incomplete. To achieve the fit of Figure 4, PV Ni II is needed for the 3900 Å absorption (one of the absorptions that is not seen distinctly in SN 1998aq; Figure 3) and PV Co II is needed for the 4000 Å absorption, but as Figure 5 shows, this part of the spectrum is not well fit with PV components alone. In Figure 5 there also is a serious lack of synthetic absorption to the right of what appears to be a sharp emission peak in the observed spectrum at 4060 Å. L01 called attention to this apparent emission feature and noted that it had not previously been observed in SNe Ia.

Figure 6 is like Figure 4 but with only the HV components in the synthetic spectrum. The HV Fe II lines play a relatively minor role and their identification is not definite, but remarkably, HV Ti II lines are important. These are the same Ti II lines that, forming at lower velocities, produce the blue trough in peculiar underluminous SN 1991bg-like SNe Ia (Filippenko et al. 1992b), in SNe Ib (Branch et al. 2002), and in SNe Ic (Millard et al. 1999). The difference between the signatures of PV Ti II, as seen in SN 1991bg-like SNe Ia, and HV Ti II, as seen in SN 2000cx, is shown in Figure 7. Note that in both cases Ti II features appear near the middle of the B band. The HV Ti II lines of SN 2000cx produce both a sudden depression of the spectrum beginning at wavelengths shorter than 4290 Å and a flux peak at 4060 Å. The previously unidentified 4060 Å peak turns out to be part of the signature of blended HV Ti II resonance-scattering features. (The identification of HV Ti II in SN 2000cx is a good example of the utility of **Synow**. It is unlikely that HV Ti II could have been recognized by looking at line lists or by performing detailed spectrum calculations for existing hydrodynamical models.) The HV Ti II features of SN 2000cx are partly responsible for the depression of the spectrum from 3900 to 4300 Å, therefore they alter the B magnitude and the $B - V$ color relative to normal SNe Ia, which do not have

significant Ti II features.

The synthetic spectrum of Figure 4 does not account for the 4530 Å absorption. We have not been able to find a plausible PV ion to account for this absorption. A transition blueshifted by about 13,000 km s⁻¹ would need to have a rest wavelength near 4720 Å. The best fit we could achieve with PV matter, without seriously degrading the fit elsewhere, would be with undetached He II λ4686, but this identification is unlikely because even with nonthermal excitation by radioactivity the appearance of He II lines is unexpected, and we would need to invoke He II forming at a lower velocity than all other PV ions except Ca II. When He II is detached to 13,000 km s⁻¹, like the other PV ions, its absorption is too blue to fit the 4530 Å absorption. The strongest optical line of C III, λ4647, is too blue even when it is undetached at 11,000 km s⁻¹. C II λ4745 detached at 15,000 km s⁻¹ could fit the 4530 Å absorption, but then C II λ6580 would produce a strong feature near 6250 Å that is not observed.

If the 4530 Å absorption is not produced by PV matter then perhaps it is produced by HV matter. A transition blueshifted by about 22,000 km s⁻¹ would need to have a rest wavelength near 4860 Å. The only plausible HV candidate that we can suggest is Hβ, at λ4861. Figure 8 shows the effect of including hydrogen lines detached at 22,000 km s⁻¹, with an optical depth of the reference line, Hα, of 5. With these parameters Hβ accounts for the 4530 Å absorption, while Hα falls within the 6110 Å absorption. At first glance the excessive depth of the synthetic Hα absorption appears to contradict the Hβ identification, but as discussed in T03, this is not necessarily the case. If HV hydrogen is in a clump that covers only a fraction of the photosphere, as inferred by T03 for the HV Ca II absorption, rather than covering all of the photosphere as assumed in a 1-D **Synow** calculation, then the fractional depth of the Hα absorption is limited by the photospheric covering fraction. This can be seen in Figure 13 of T03, where Hβ and Hα are simultaneously fit reasonably well by a model in which hydrogen is confined to a HV clump with a low photospheric covering fraction.

Since we have not found a plausible alternative to Hβ, forming at *any* velocity between 13,000 and 22,000 km s⁻¹, in the remainder of this article we will use Hβ to account for the 4530 Å absorption. We will return to the issue of Hα, and consider the Paschen lines, in §5.1 and §5.2.

4. LATER SPECTRA

In this section we more briefly discuss the day 7, day 15, and day 32 spectra. At each epoch we compare the spectrum of SN 2000cx with (1) a spectrum of SN 1998aq; (2) an earlier-epoch spectrum of SN 2000cx; and (3) a synthetic spectrum.

4.1. The Day 7 Spectrum

The day 7 spectrum of SN 2000cx is compared with a day 7 spectrum of SN 1998aq in Figure 9. The differences remain substantial and generally similar to those of day 2. Again the suppression of the blue part of the spectrum and the weaker S II lines cause the $B - V$ color of SN 2000cx to be redder than that of SN 1998aq.

The day 7 and day 2 spectra of SN 2000cx are compared in Figure 10. The wavelengths of the absorptions are very similar. The most significant difference is that the day 7 spectrum has developed more prominent peaks near 4450 and 5170 Å, with the latter apparently partly filling in the 5270 Å absorption.

Figure 11 shows a comparison of the day 7 spectrum with a synthetic spectrum that has $v_{phot}=11,000$ km s⁻¹, $T_{bb} = 10,000$ K, and contains lines of the same ten ions as in Figure 8 (including H I). The ion-specific input parameters are listed in Table 2. Again all PV ions except Ca II are mildly detached at 13,000 km s⁻¹. Comparing Tables 1 and 2, we see that the reference-line optical depths have changed only mildly. The increase in the Fe III optical depth and the decrease in the S II optical depth are responsible for getting reasonable fits to the 4450 and 5170 Å peaks. At day 7 the synthetic spectrum in the blue still is a composite of PV and HV line formation.

4.2. The Day 15 Spectrum

The day 15 spectrum of SN 2000cx is compared with a day 18 spectrum of SN 1998aq in Figure 12. Except at the red end, the spectra still are very different. In fact, at wavelengths shorter than about 4600 Å the spectra are practically opposite: SN 2000cx has absorptions where SN 1998aq has peaks. The spectra differ so much in the B and V bands that any close similarity of their $B - V$ colors would be accidental.

The day 15 and day 7 spectra of SN 2000cx are compared in Figure 13. At day 15 the 6110 Å absorption has hardly changed, but a broad absorption has developed at 5670 Å and the S II absorptions no longer can be seen. The 4530 Å absorption is still present, now to

the left of an emission peak that has emerged at 4580 Å.

Figure 14 shows a comparison of the day 15 spectrum with a synthetic spectrum that has $v_{phot}=10,000$ km s⁻¹, $T_{bb} = 12,000$ K, and contains lines of seven ions: Na I, Si II, Fe II, Fe III, and Co II have PV components; H I and Ti II are at HV. At this epoch Mg II, S II, and Ni II lines are no longer being used. The ion-specific input parameters are listed in Table 3. The broad 5670 Å absorption is well fit by the Na I D lines ($\lambda\lambda 5890, 5896$) with a high value of $v_e = 7$. The spectrum at wavelengths shorter than 5000 Å also is well fit. This has been accomplished by retaining the Fe III lines and by introducing Fe II lines having a significant optical depth throughout the whole velocity interval of 11,000 to 23,000 km s⁻¹ (by using a high e-folding velocity of $v_e = 20,000$ km s⁻¹). The development of the Fe II features causes the emergence of the 4580 Å peak. The large differences between the spectra of SNe 2000cx and 1998aq at this epoch are due to the persistent Fe III features and to Fe II features forming throughout the wide velocity interval.

4.3. The Day 32 Spectrum

The day 32 spectrum of SN 2000cx is compared with a day 32 spectrum of SN 1998aq in Figure 15. At this epoch the spectra generally contain the same features, but those in the blue remain more blueshifted in SN 2000cx. Both L01 and C03 emphasized that SN 2000cx violates the “Lira–Phillips” law (Lira 1995; Phillips et al. 1999) — that the extinction-corrected $B - V$ color of SNe Ia evolves in an uniform way from day 30 to day 90. Throughout this time interval SN 2000cx is anomalously blue. It is clear from Figure 15 that in addition to whatever peculiarity there may be in the underlying continuum (or pseudo-continuum), the higher blueshifts of the features in SN 2000cx play a role in altering the $B - V$ color at day 32.

The day 32 and day 15 spectra of SN 2000cx are compared in Figure 16. At day 32 the overall energy distribution is much redder. The 6110 Å absorption is still present but flanked by absorptions at 6000 and 6280 Å that are commonly attributed to Fe II. L01 pointed out that these Fe II features were unusually late to develop in SN 2000cx. At wavelengths shorter than about 5400 Å the spectrum has changed dramatically: broad absorptions appear near 5100 Å and 4400 Å, where emission peaks appeared at day 15. The 4530 Å absorption no longer is seen, although its presence on the steep blue side of the 4600 Å peak is difficult to exclude.

Figure 17 shows a comparison of the day 32 spectrum with a synthetic spectrum that has $v_{phot}=11,000$ km s⁻¹, $T_{bb} = 8000$ K, and contains lines of Na I, Si II, Ca II, and Fe II at

PV, and only Ca II at HV. H I and Fe III lines are no longer used. The ion-specific input parameters are listed in Table 4. Apart from the three features labelled in Figure 17, all of the synthetic features are due to Fe II. As we did for the late photospheric spectra of SN 1991T (Fisher et al. 1999) and of the SN 1991T-like event SN 1997br (Hatano et al. 2002), we have introduced a discontinuity in the Fe II optical depth. It decreases exponentially from 100 at $v_{phot} = 11,000 \text{ km s}^{-1}$ to 37 at $v = 13,000 \text{ km s}^{-1}$; there it abruptly falls to 2 and then decreases exponentially again. The broad 5100 and 4400 Å absorptions are formed in the high optical-depth region, which we interpret as the outer part of an iron-rich core. (In SNe 1991T and 1997br we placed the discontinuity at 10,000 and 12,500 km s^{-1} , respectively.) The differences between SNe 2000cx and 1998aq in Figure 17 are mainly caused by Fe II line formation extending to higher velocities, and to deep HV Ca II, in SN 2000cx.

5. PREMAXIMUM SPECTRA

In this section we turn our attention to the premaximum spectra: the optical day -3 spectrum and the infrared day -5.5 spectrum.

5.1. The Day -3 Spectrum

The day -3 spectrum of SN 2000cx is compared with a day -3 spectrum of SN 1998aq in Figure 18. The difference in the blue is qualitatively like at day 2, but even more extreme.

The day -3 and day 2 spectra of SN 2000cx are compared in Figure 19. The day -3 spectrum has a distinct absorption feature at 4370 Å and a weaker one at 5510 Å both of which are weak or absent in the day 2 spectrum. Otherwise, the same spectral features are present but at different strengths: at day -3 the S II features are much weaker and the spectrum in the blue is even more suppressed than at day 2.

Figure 20 shows a comparison of the day -3 spectrum with a synthetic spectrum that has $v_{phot}=12,000 \text{ km s}^{-1}$, $T_{bb} = 9000 \text{ K}$, and contains lines of nine ions: the same as in Figure 7 for the day 2 spectrum except that PV Co II has been omitted and PV Si III has been added. The ion-specific input parameters are listed in Table 5. The 4370 Å absorption is accounted for by Si III $\lambda 4550$. L01 suggested that the 5510 Å absorption could be Si III $\lambda 5740$. We believe this to be correct, because although the synthetic spectrum of Figure 20 does not produce the feature, if we make $\lambda 4550$ somewhat too strong then $\lambda 5740$ does account for the 5510 Å absorption. At this epoch Ti II is blocking the blue flux even more than at day 2, and again producing a 4060 Å peak.

In the day -3 spectrum of SN 2000cx, the shape of the feature near 6100 \AA is similar to its shape in SNe 1991T and 1997br (L01). This line shape, with its steep blue edge and nearly horizontal part extending from about 6100 \AA to 6300 \AA , has been thought to be odd. But the reason the shape looks odd is that the line is rather weak and superimposed on a strongly sloping continuum. When the spectrum is tilted to make the underlying continuum relatively flat, the line profile looks like that of a normal resonance-scattering feature. The resemblance of this feature in SN 2000cx to the same feature in SNe 1991T and 1997br, in which no conspicuous “H β ” features are seen, suggests that there is little room for an H α contribution to the spectrum of SN 2000cx at this epoch. But as discussed in T03, if H α is confined to a clump in front of the photosphere and its source function is higher than that of resonance scattering as it ordinarily is in SNe II, it may be hard to see. (In the special case that its source function equals the intensity from the photosphere, the spectroscopic signature of H α confined to a clump in front of the photosphere would vanish.)

5.2. The Day -5.5 Infrared Spectrum

Figure 21 shows a comparison of the short wavelength part of the day -5.5 infrared spectrum, obtained by R02, with a straightforward extension of the optical synthetic spectrum of Figure 21, for day -3 . The PV Mg II features in the synthetic spectrum may have counterparts in the observed spectrum but the synthetic features are too strong, possibly due to the mismatch of epochs if the Mg II optical depth is increasing with time. The most important point is that the $1.02 \mu\text{m}$ absorption cannot be due to Mg II $\lambda 10926$ forming above $20,000 \text{ km s}^{-1}$, as assumed in R02, because Mg II $\lambda 9226$ blueshifted by $20,000 \text{ km s}^{-1}$ would produce a strong absorption at 8600 \AA , near a peak in the observed spectrum. In LTE Mg II $\lambda 9226$ has a higher optical depth than Mg II $\lambda 10926$ for any reasonable excitation temperature. The Mg II $\lambda 10926$ and $\lambda 9226$ absorptions do appear to be present in other SNe Ia, but at lower velocities ranging from about $11,000$ to $15,000 \text{ km s}^{-1}$ (Marion et al. 2003).

Figure 21 also presents the same synthetic spectrum, but including He I lines detached at $21,000 \text{ km s}^{-1}$. This shows that HV He I $\lambda 10830$ could be responsible for at least the core of the $1.02 \mu\text{m}$ absorption. If the HV matter contains hydrogen then it also contains helium, although nonthermal excitation would be required to produce a significant optical depth in He I $\lambda 10830$. R02 mentioned that He I $\lambda 20581$ is not present in their spectra, but detailed calculations will be required to determine whether this is inconsistent with the presence of He I $\lambda 10830$.

In the synthetic spectrum of Figure 21 hydrogen P β is so weak that it provides no evi-

dence for or against the presence of $H\beta$ in SN 2000cx. When extended to longer wavelengths the synthetic spectrum for day -3 does contain a weak blueshifted hydrogen $P\alpha$ absorption component that is not seen in the observed spectrum, but $P\alpha$, like $H\alpha$, may have an elevated source function with respect to resonance scattering, and be difficult to see when confined to a clump.

6. DISCUSSION

We have found that in the blue the early photospheric-phase spectra of SN 2000cx are composite, containing not only relatively high-excitation features just above the photospheric velocity (PV) of $\sim 10,000 \text{ km s}^{-1}$, but also lower-excitation features forming at much higher velocity (HV), above $\sim 20,000 \text{ km s}^{-1}$. It is clear that the HV features are partly responsible for the photometric peculiarities of SN 2000cx. For example, HV Ti II features are present in the B band. For the day -3 , 2, 7, 15, and 32 synthetic spectra we have used Ti II reference-line optical depths of 0.7, 0.4, 0.6, 0.3, and 0.0, respectively, not inconsistent within our fitting freedom with a smoothly decreasing Ti II optical depth. Other things being equal, the decreasing blocking of blue flux by HV Ti II lines would cause the B band to rise more quickly than normal, and then to decline more slowly than normal. This is likely to be at least partly responsible for the lopsided B -band light curve. In our present 1-D calculations, most of the flux removed by Ti II absorption features tends to be re-emitted just to the red, still in the B band. But if Ti II lines form in a clump in front of the photosphere, then the absorbed flux is emitted into all directions and the observer sees strong net absorption. Thus quantitatively evaluating the effects of HV line formation on photometry is a task for 3-D calculations.

Similarly, the presence of HV Ca II infrared triplet absorption in the I band may be partly responsible for the unusual behavior of the I -band light curve discussed by L01 and C03. We can see from Figs. 1, 15, and 17 that HV Ca II remains strong even as late as day 32. The evolution of the line strengths of clump-confined matter can be complex, reflecting not only the usual Sobolev t^{-2} optical-depth decline for homologous expansion, and whatever excitation and ionization changes may occur, but also the evolving fraction of the photosphere that is covered by the clump. When the photosphere recedes with respect to the homologously expanding matter an increasing fraction of the photosphere may be covered by the clump.

The only plausible identification that we can find for the 4530 \AA absorption is HV $H\beta$. This identification is tentative, however, because there is no supporting evidence, and the lack of a conspicuous $H\alpha$ signature at day -3 may require fine tuning of the $H\alpha$ source

function.

The origin of the HV matter in SN 2000cx remains unclear. If the HV matter consists of unburned carbon and oxygen with solar abundances of heavier elements, then the required HV mass of $\sim 10^{-3} M_{\odot}$ could be contained in a HV clump of ejecta (T03). But if the HV matter is hydrogen-rich then it must have come from a nondegenerate companion star (Marietta, Burrows, & Fryxell 2000), because $10^{-3} M_{\odot}$ of hydrogen could not have been present on the surface of the progenitor white dwarf without burning. From the absence of a narrow circumstellar H α feature in early high-resolution spectra, Lundqvist et al. (2003) infer an upper limit to the wind mass-loss rate of the companion of $\sim 10^{-5} M_{\odot} \text{ yr}^{-1}$.

The PV spectra of SN 2000cx also are peculiar. After allowing for the now-recognized role of HV Ti II features in the blue, the case for a spectroscopic relation between the underlying PV spectra of SNe 2000cx and 1991T is perhaps strengthened. We confirm and extend the findings of L01 that Fe III lines persisted for an unusually long time after maximum, that line blueshifts were higher than normal, and that Fe II lines were late to develop. We find that when Fe II lines finally did develop during the late photospheric phase, they formed out to higher velocities than in normal SNe Ia. All of this seems consistent with the suggestion by L01 that SN 2000cx was a more powerful version of SN 1991T, but as emphasized by C03, a reliable distance to NGC 524 is needed to determine the luminosity of SN 2000cx.

Although HV line formation is unusually strong in SN 2000cx, it has become clear that it sometimes occurs in other SNe Ia. HV Ca II and Fe II were first recognized in premaximum spectra of SN 1994D (Hatano et al. 1999a); strong signatures of HV Ca II have been detected in premaximum flux and polarization spectra of SN 2001el (Wang et al. 2003; Kasen et al. 2003); HV Ca II can be seen in premaximum spectra of SNe 1999ee (Hamuy et al. 2002; P. Mazzali, in preparation); and HV Fe II has been invoked to fit both premaximum and postmaximum spectra of SN 1998aq (B03). Recently Gerardy et al. (2003) have attributed HV Ca II in SN 2003du to a dense shell formed by interaction of the high-velocity ejecta with $\sim 2 \times 10^{-2} M_{\odot}$ of hydrogen-rich circumstellar matter. Further close scrutiny of SN Ia spectra to look for more subtle signs of HV line formation is needed. An indication of which ions would be likely to appear at various temperatures, for carbon-oxygen rich and hydrogen rich compositions, can be obtained from Figs. 11 and 12 of T03. These figures show that (in LTE) when H, Ca II, Ti II, and Fe II are present, additional possibilities include Na I, Fe I, Sr II, and Ba II, depending on the temperature and electron density.

The “H β ” feature of SN 2000cx has never been seen, or at least never recognized, in other SNe Ia. If the HV H β identification in SN 2000cx is correct, and yet HV H β seldom if ever appears in the spectra of other SNe Ia, even those that exhibit HV Ca II features,

one reason could be that the outer layers of most donor stars in SN Ia binary progenitor systems are helium-rich rather than hydrogen-rich (e.g., Kato & Hachisu 2003 and references therein).

Hamuy et al. (2003) have discovered a hydrogen signature in SN 2002ic that differs from the putative clump-confined HV hydrogen associated with SN 2000cx. The $H\alpha$ emission associated with SN 2002ic has a characteristic velocity of only $\sim 1800 \text{ km s}^{-1}$. It is unlikely that this kind of circumstellar hydrogen signature would have gone unrecognized in previously observed SNe Ia, so it appears that SN 2002ic, although very interesting, is a special case.

This work has been supported by NSF grants AST-9986965, AST-0204771, and AST-0307323, NASA grant NAG 5-12127, and grant HST-AR-09544-01A (provided by NASA through the STScI, operated by AURA Incorporated, under NASA contract NAS5-26555). RJR was supported by The Aerospace Corporation's Independent Research and Development Program.

REFERENCES

- Boffi, F. R., & Riess, A. G. 2003, in *Symbiotic Stars Probing Stellar Evolution*, ed. R. L. M. Coradi, J. Mikolajewska, & T. J. Mahoney (San Francisco, ASP), in press
- Branch, D., et al. 2002, *ApJ*, 566, 1005
- Branch, D., et al. 2003, *AJ*, 126, 1489 (B03)
- Candia, P., et al. *PASP*, 115, 277 (C03)
- Filippenko, A. V. 1997, *ARAA*, 35, 309
- Filippenko, A. V. et al. 1992a, *ApJ*, 384, L15
- Filippenko, A. V. et al. 1992b, *AJ*, 105, 1543
- Fisher, A., Branch, D., Hatano, K., & Baron, E. 1999, *MNRAS*, 304, 67
- Gerardy, C. L., et al. 2003, *ApJ*, submitted; (astro-ph/0309639)
- Goldhaber, G., et al. 2001, *ApJ*, 558, 359
- Hamuy, M., et al. 2002, *AJ*, 124, 417
- Hamuy, M., et al. 2003, *Nature*, 424, 651
- Hatano, K., Branch, D., Fisher, A., Baron, E., & Filippenko, A. V. 1999a, *ApJ*, 525, 881
- Hatano, K., Branch, D., Fisher, A., Millard, J., & Baron, E. 1999b, *ApJS*, 121, 233
- Hatano, K., Branch, D., Qiu, Y. L., Baron, E., Thielemann, F.-K., & Fisher, A. 2002, *New Astr.*, 7, 441
- Kasen, D., et al. 2003, *ApJ*, 593, 788
- Kato, M., & Hachisu, I. 2003, *ApJ*, 598, L107
- Lentz, E. J., Baron, E., Branch, D., & Hauschildt, P. H. 2001, *ApJ*, 557, 266
- Li, W. et al. 2001, *PASP*, 113, 1178 (L01)
- Lira, P. 1995, Masters thesis, Univ. Chile
- Lundqvist, P., Sollerman, J., Leibundgut, B., Baron, E., Fransson, K., & Nomoto, K. 2003, in *From Twilight to Highlight: The Physics of Supernovae*, ed. W. Hillebrandt & B. Leibundgut (Berlin: Springer), p. 309
- Marietta, E., Burrows, A., & Fryxell, B. 2000, *ApJS*, 128, 615
- Marion, G. H., Höflich, P., Vacca, W. D., & Wheeler, J. C. 2003, *ApJ*, 591, 316
- Meikle, W. P. S., et al. 1996, *MNRAS*, 281, 263
- Millard, J., et al. 1999, *ApJ*, 527, 746

- Perlmutter, S., et al. 1997, ApJ, 483, 565
- Phillips, M. M., Lira, P., Suntzeff, N. B., Schommer, R. A., Hamuy, M., & Maza, J. 1999, AJ, 118,1766
- Riess, A. G., Press, W. H., & Kirshner, R. P. 1996, ApJ, 473, 88
- Rudy, R. J., Lynch, D. K., Mazuk, S., Venturini, C. C., Puetter, R. C., & Höflich, P. 2002, ApJ, 565, 413 (R02)
- Thomas, R. C., Branch, D., Baron, E., Nomoto, K., Li, W., & Filippenko, A. V. 2003, ApJ, in press (astro-ph/0302260; T03)
- Wang, L., et al. 2003, ApJ, 591, 1110
- Wheeler, J. C., Höflich, P., Harkness, R. P., & Spyromilio, J. 1998, ApJ, 496, 908

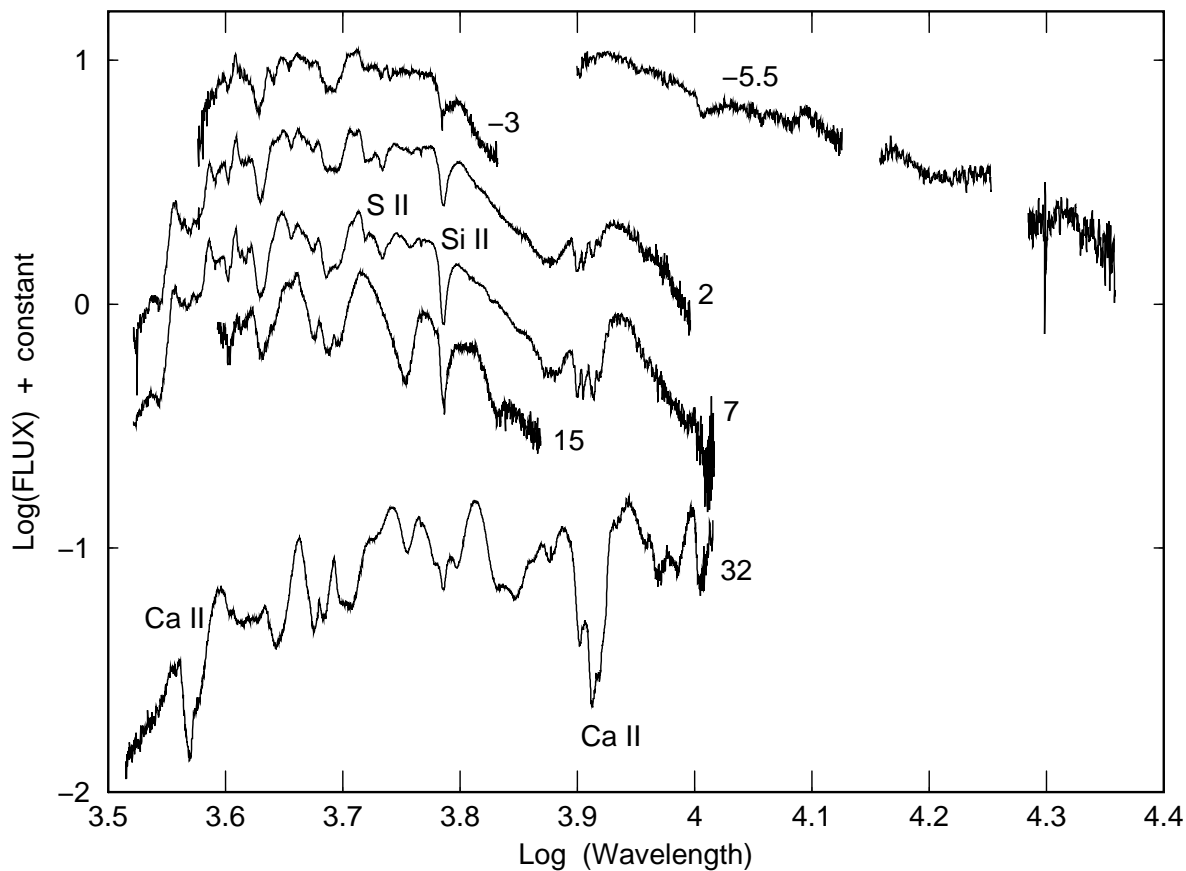


Fig. 1.— Five optical spectra of SN 2000cx from L01 and an infrared spectrum from R02 are displayed. Epochs are in days with respect to the date of maximum brightness in the *B* band, 2000 July 27 (L01). The IR spectrum is the sum of spectra obtained 5 and 6 days before maximum; in regions of very strong telluric absorption the IR spectrum is not plotted, and the noise near $\log(\lambda)=4.3$ is an artifact of the correction for telluric CO_2 absorption. The flux of all spectra is per unit frequency interval and the vertical displacement is arbitrary. All spectra shown in this article have been corrected for the redshift of NGC 524, $z = 0.008$. No correction for interstellar reddening has been applied.

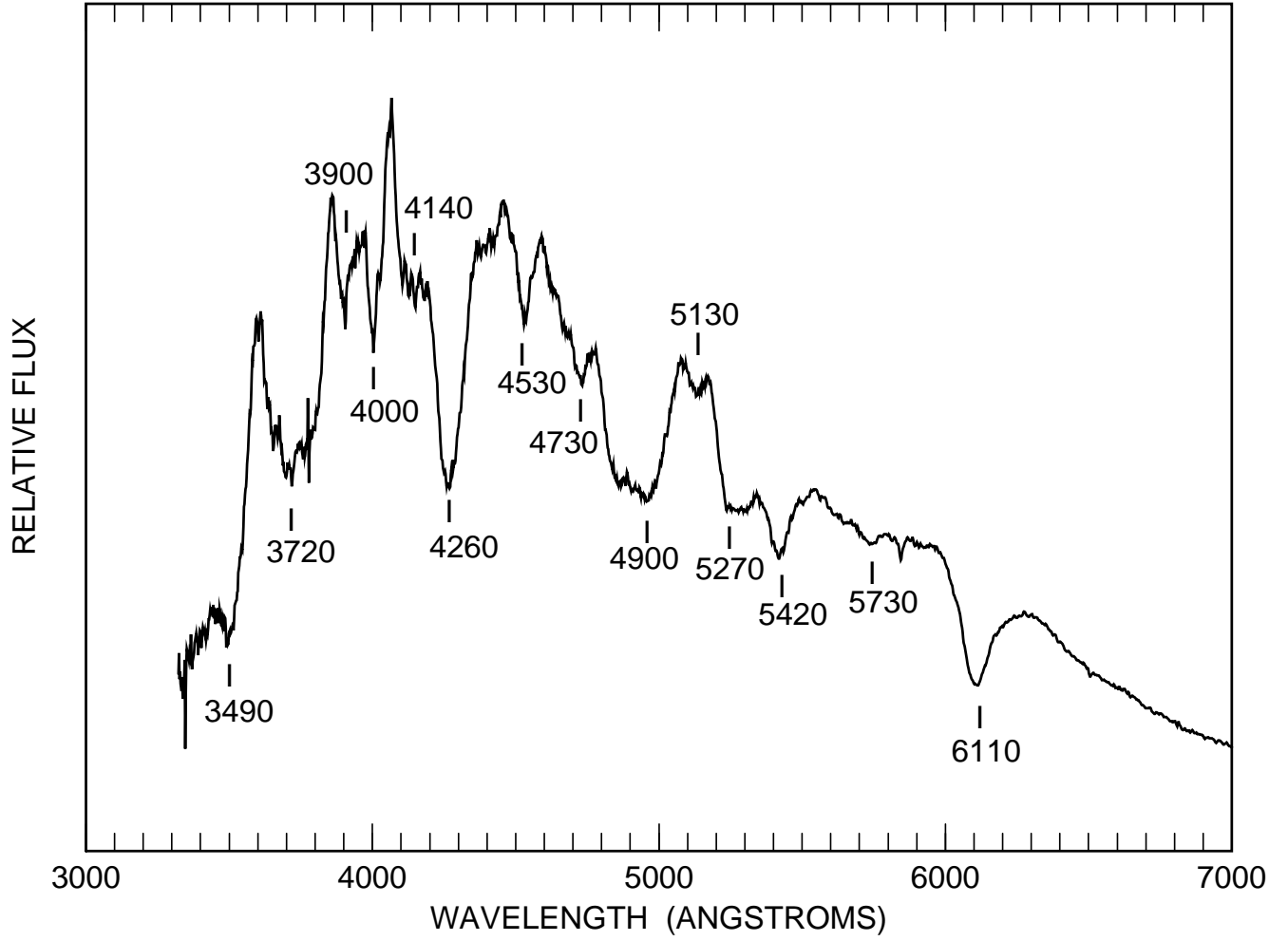


Fig. 2.— Wavelengths of absorption features in the day 2 spectrum of SN 2000cx are labelled. In this and subsequent figures the flux is per unit wavelength interval.

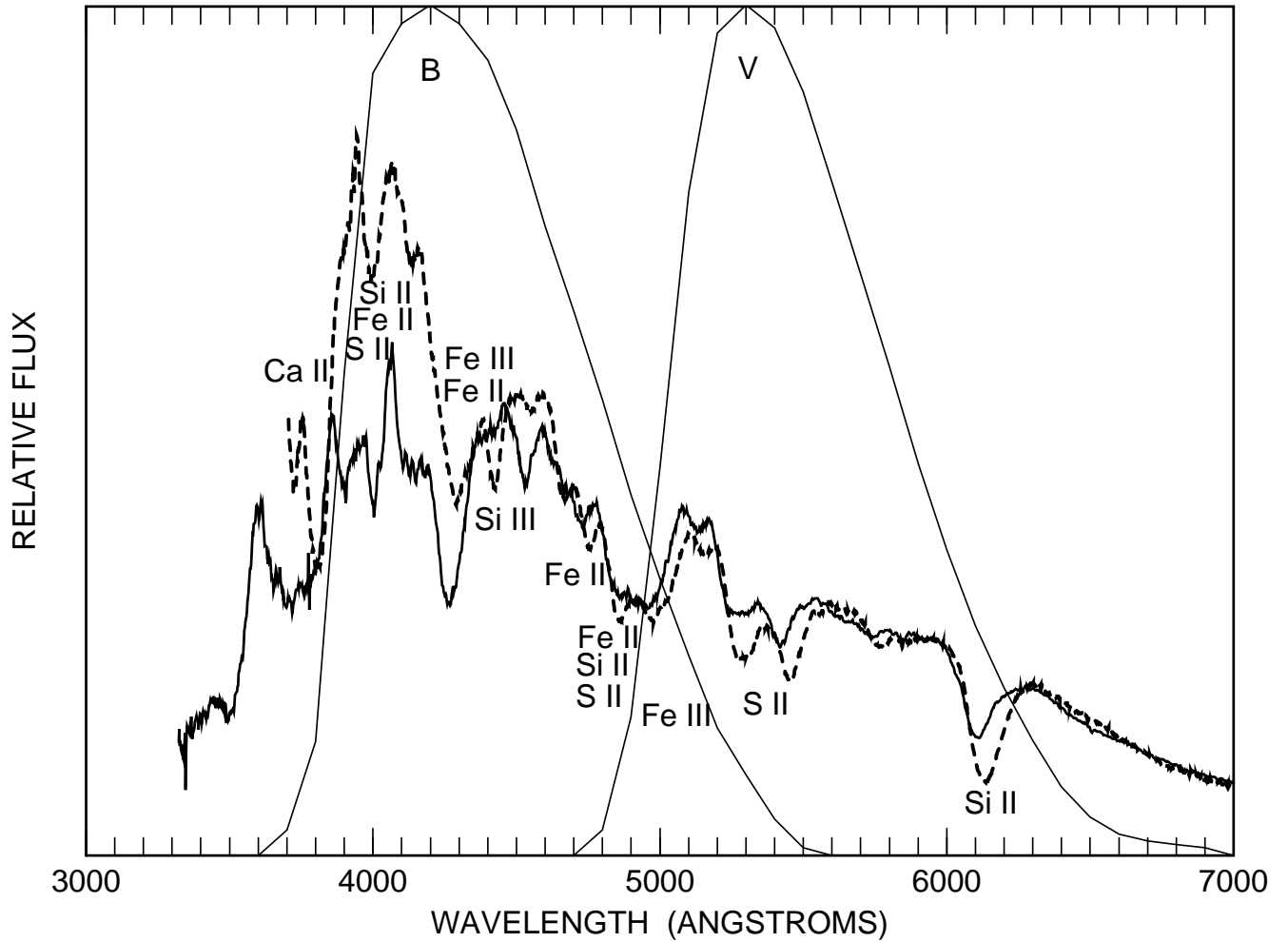


Fig. 3.— The day 2 spectrum of SN 2000cx (*thick solid line*) is compared with a day 2 spectrum of the normal SN Ia 1998aq (*dashed line*). Ions used by B03 to account for the absorption features of SN 1998aq are indicated. The *B*-band and *V*-band filter functions are also shown (*thin solid lines*).

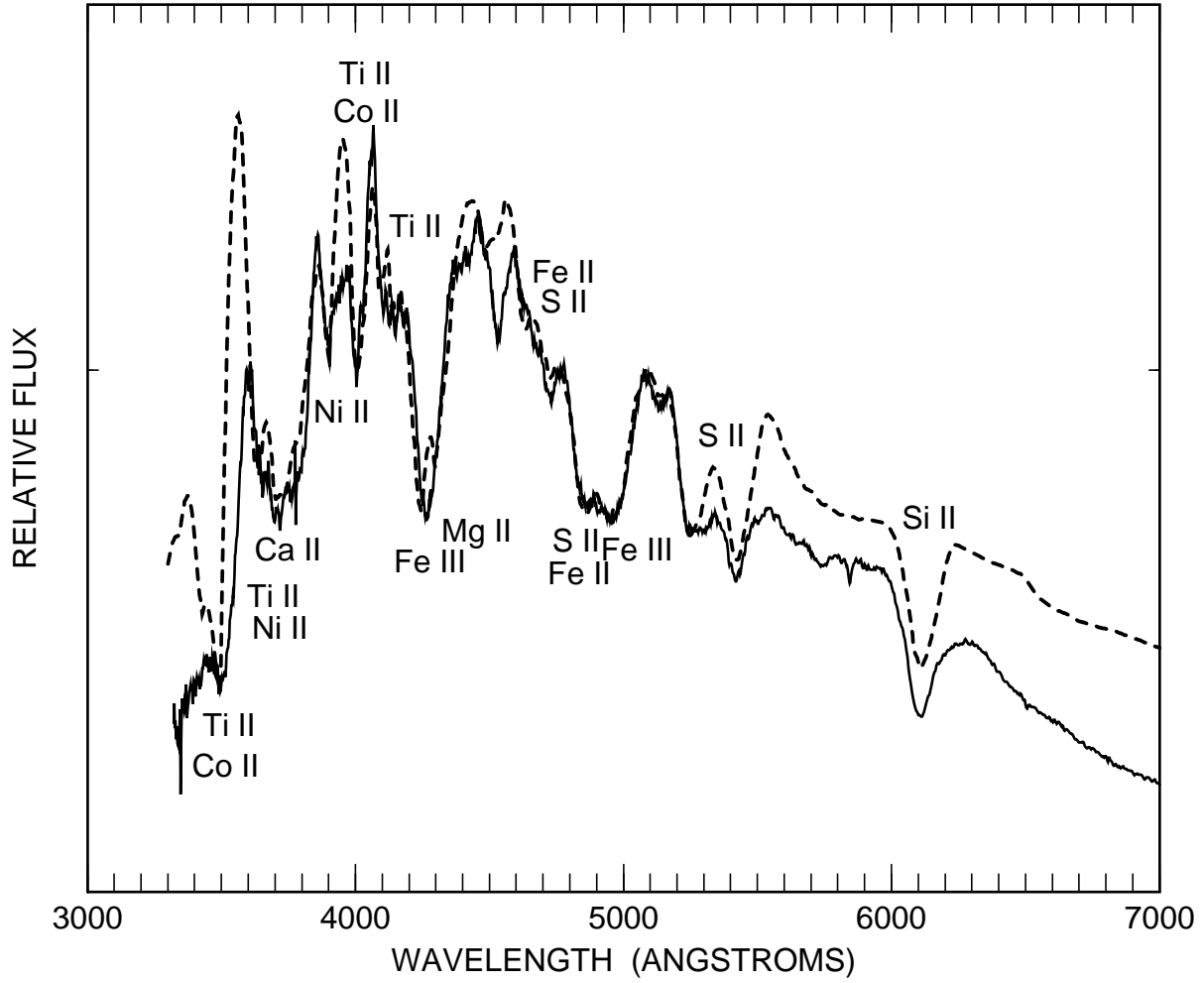


Fig. 4.— The day 2 spectrum of SN 2000cx (*solid line*) is compared with a synthetic spectrum (*dashed line*) that has $v_{phot} = 11,000 \text{ km s}^{-1}$, $T_{bb} = 9000 \text{ K}$, and contains lines of nine ions.

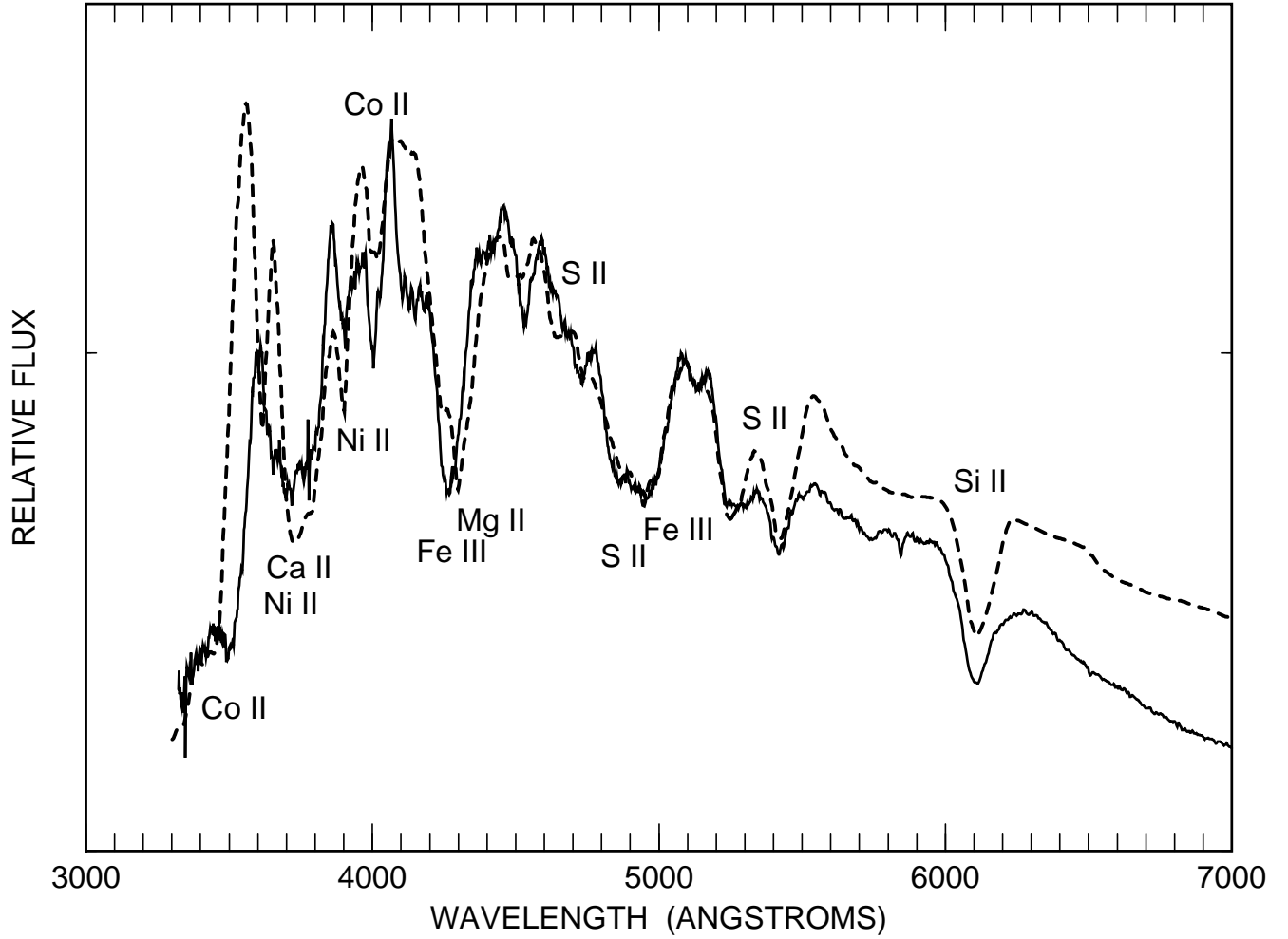


Fig. 5.— Like Figure 4 but the synthetic spectrum includes only PV line formation.

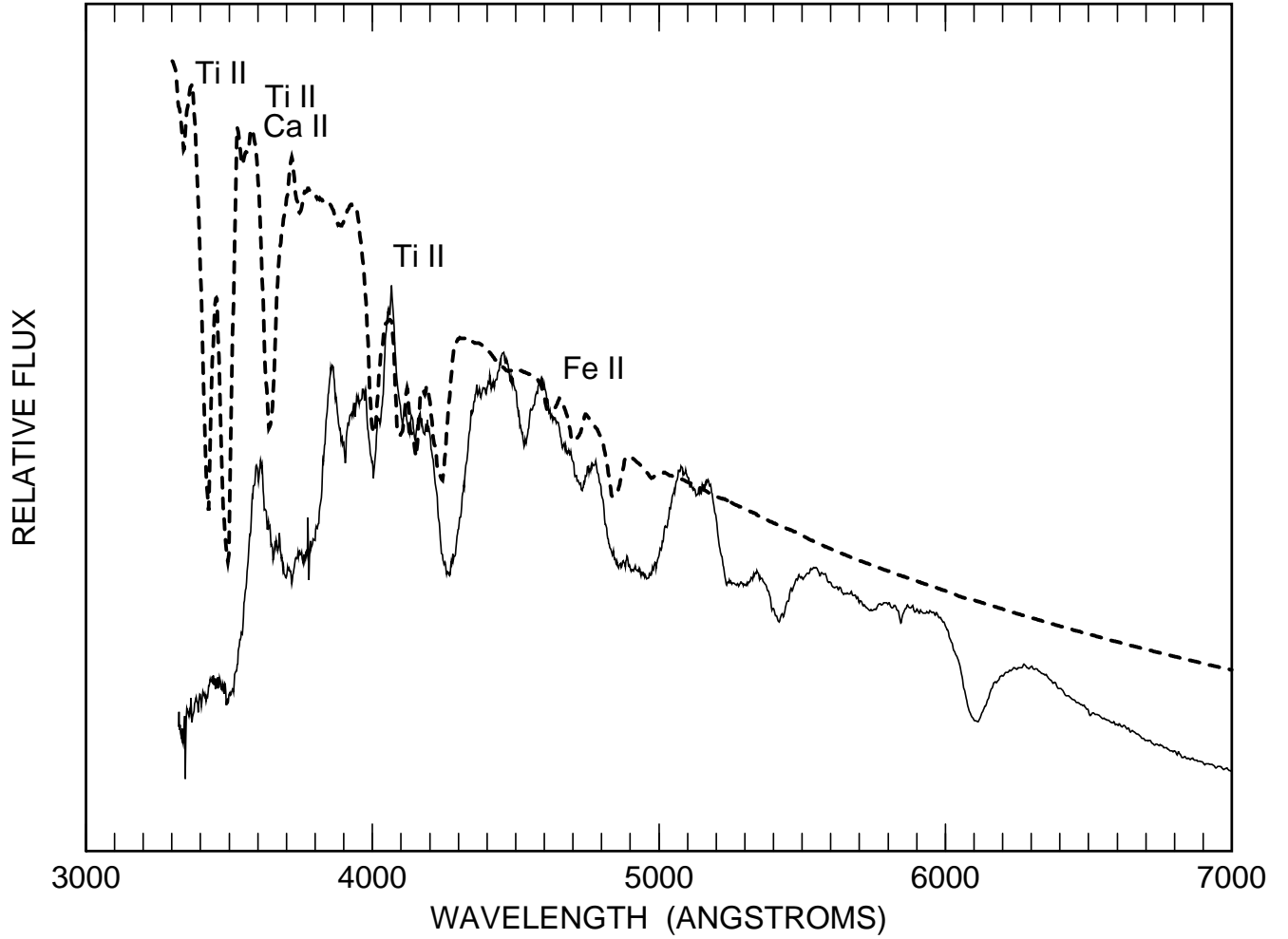


Fig. 6.— Like Figure 4 but the synthetic spectrum includes only HV line formation.

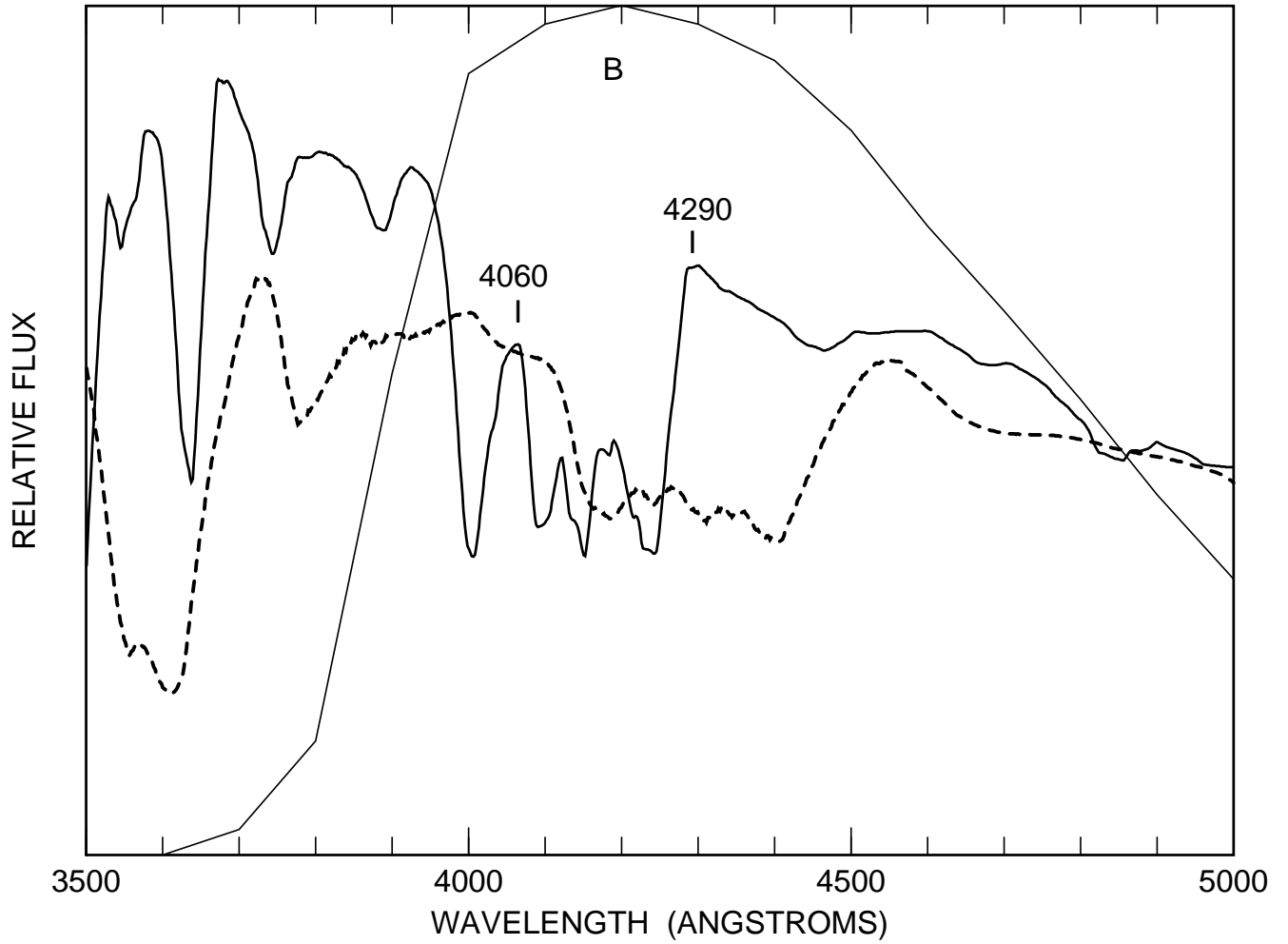


Fig. 7.— A synthetic spectrum having $v_{phot} = 11,000 \text{ km s}^{-1}$ and containing only Ti II lines detached at $23,000 \text{ km s}^{-1}$ (*solid line*) is compared with a synthetic spectrum having $v_{phot} = 11,000 \text{ km s}^{-1}$ and containing only undetached Ti II lines (*dashed line*). The *B*-band filter function is also shown (*thin solid line*).

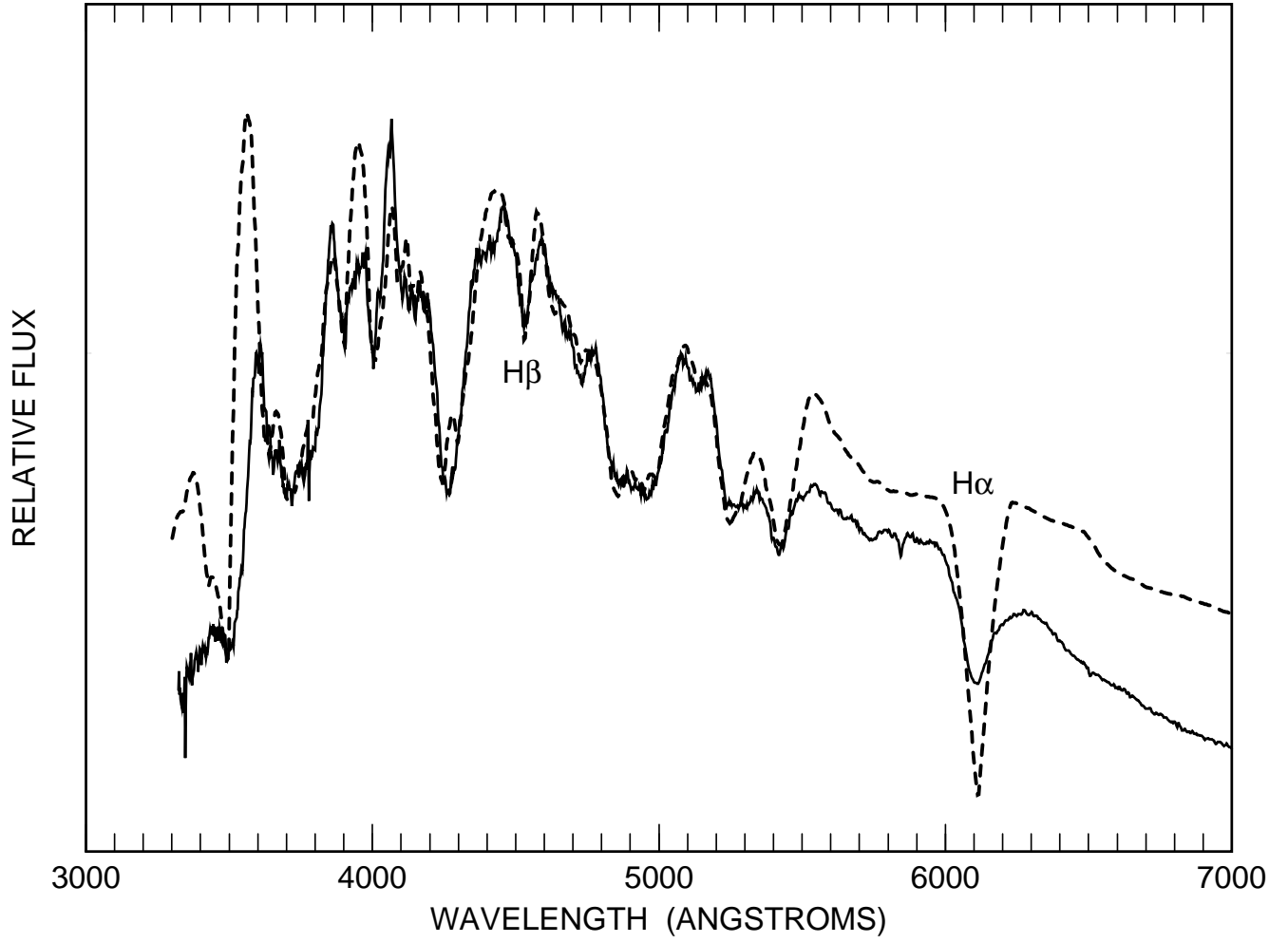


Fig. 8.— Like Figure 4 but with hydrogen lines, detached at $22,000 \text{ km s}^{-1}$, in the synthetic spectrum.

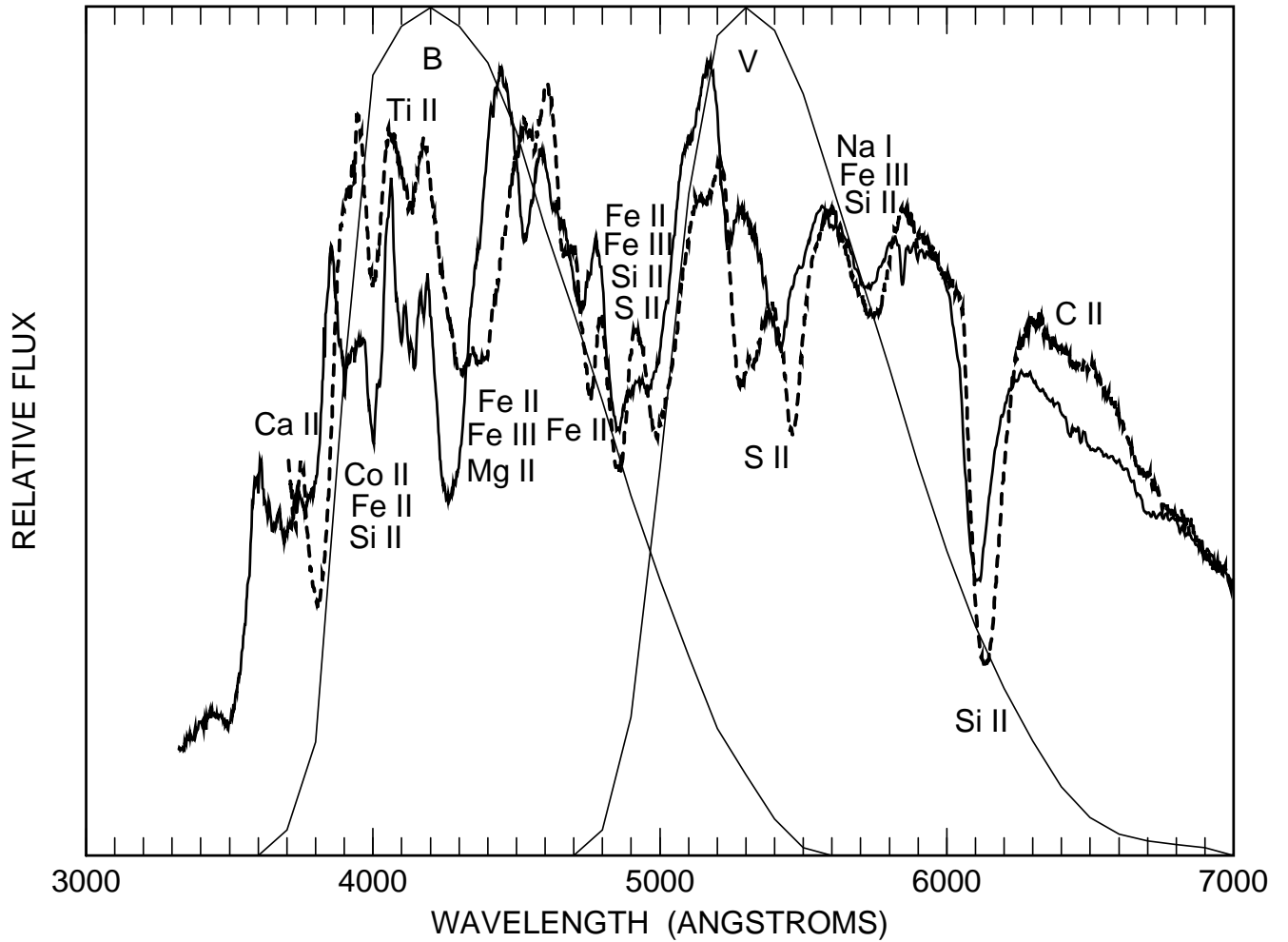


Fig. 9.— The day 7 spectrum of SN 2000cx (*thick solid line*) is compared with a day 7 spectrum of the normal SN Ia 1998aq (*dashed line*). Ions used by B03 to account for the absorption features of SN 1998aq are indicated. The *B*-band and *V*-band filter functions are also shown (*thin solid lines*).

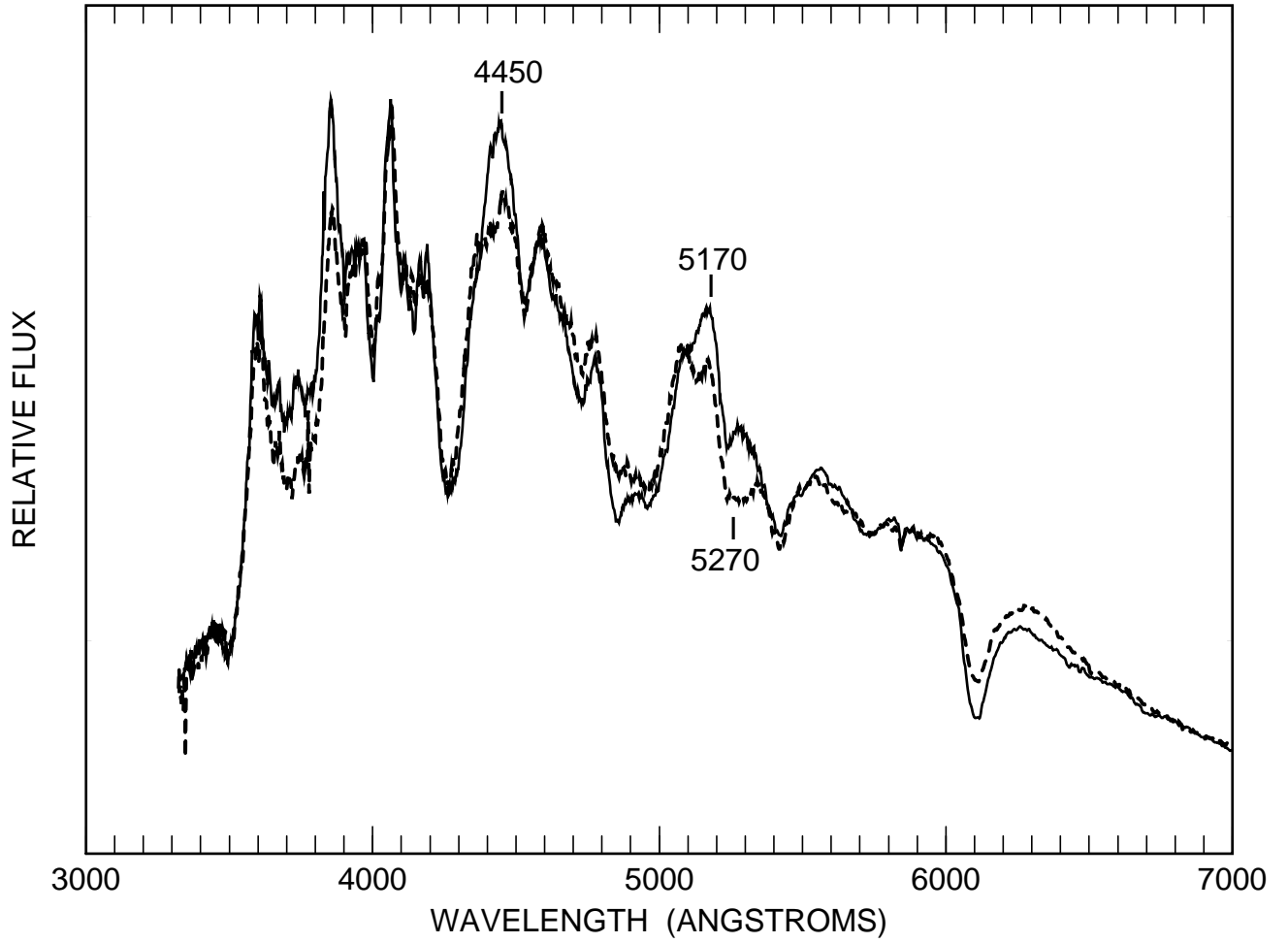


Fig. 10.— The day 7 (*solid line*) and day 2 (*dashed line*) spectra of SN 2000cx are compared.

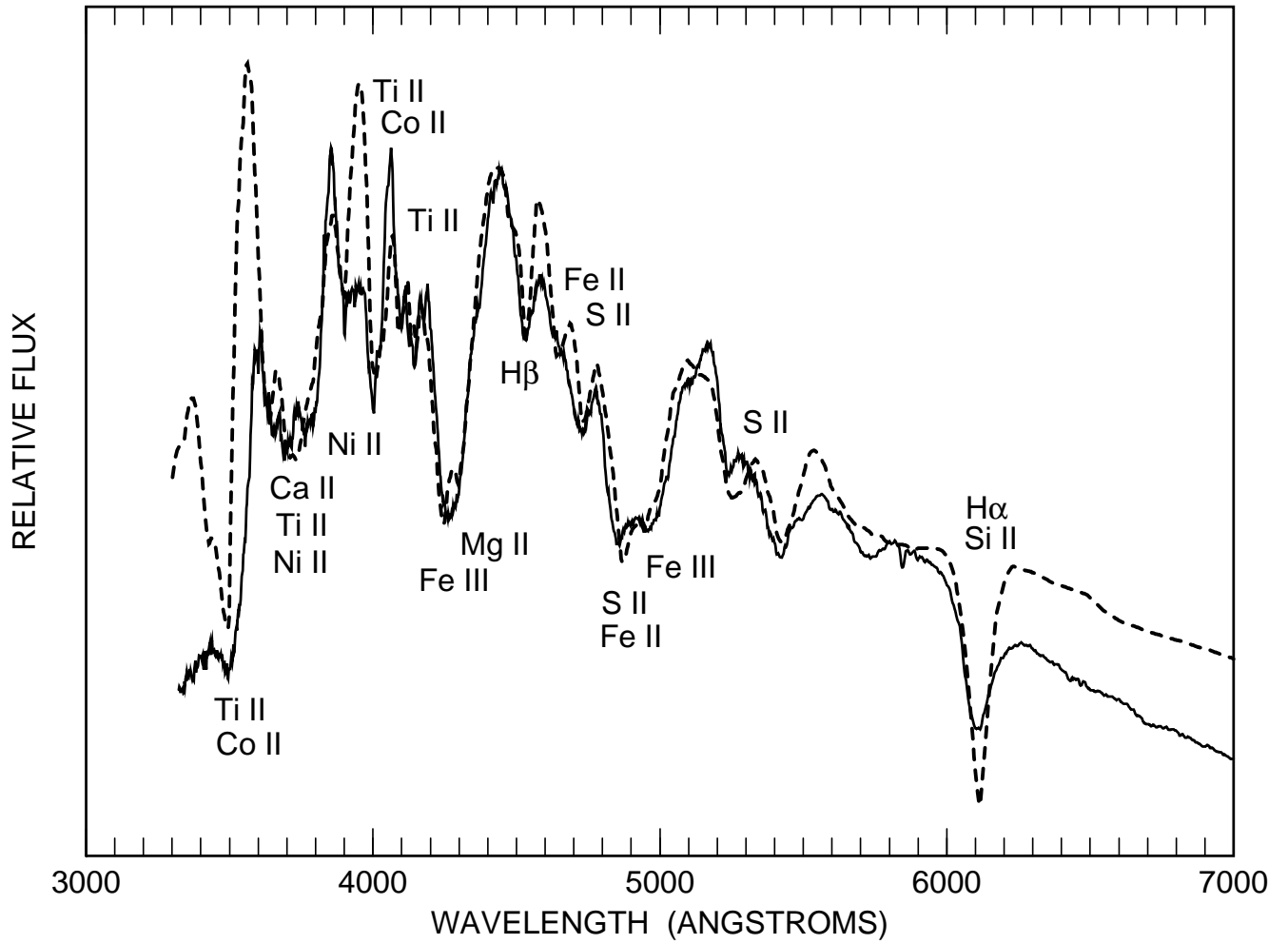


Fig. 11.— The day 7 spectrum of SN 2000cx (*solid line*) is compared with a synthetic spectrum (*dashed line*) that has $v_{phot} = 11,000 \text{ km s}^{-1}$, $T_{bb} = 11000 \text{ K}$, and contains lines of nine ions.

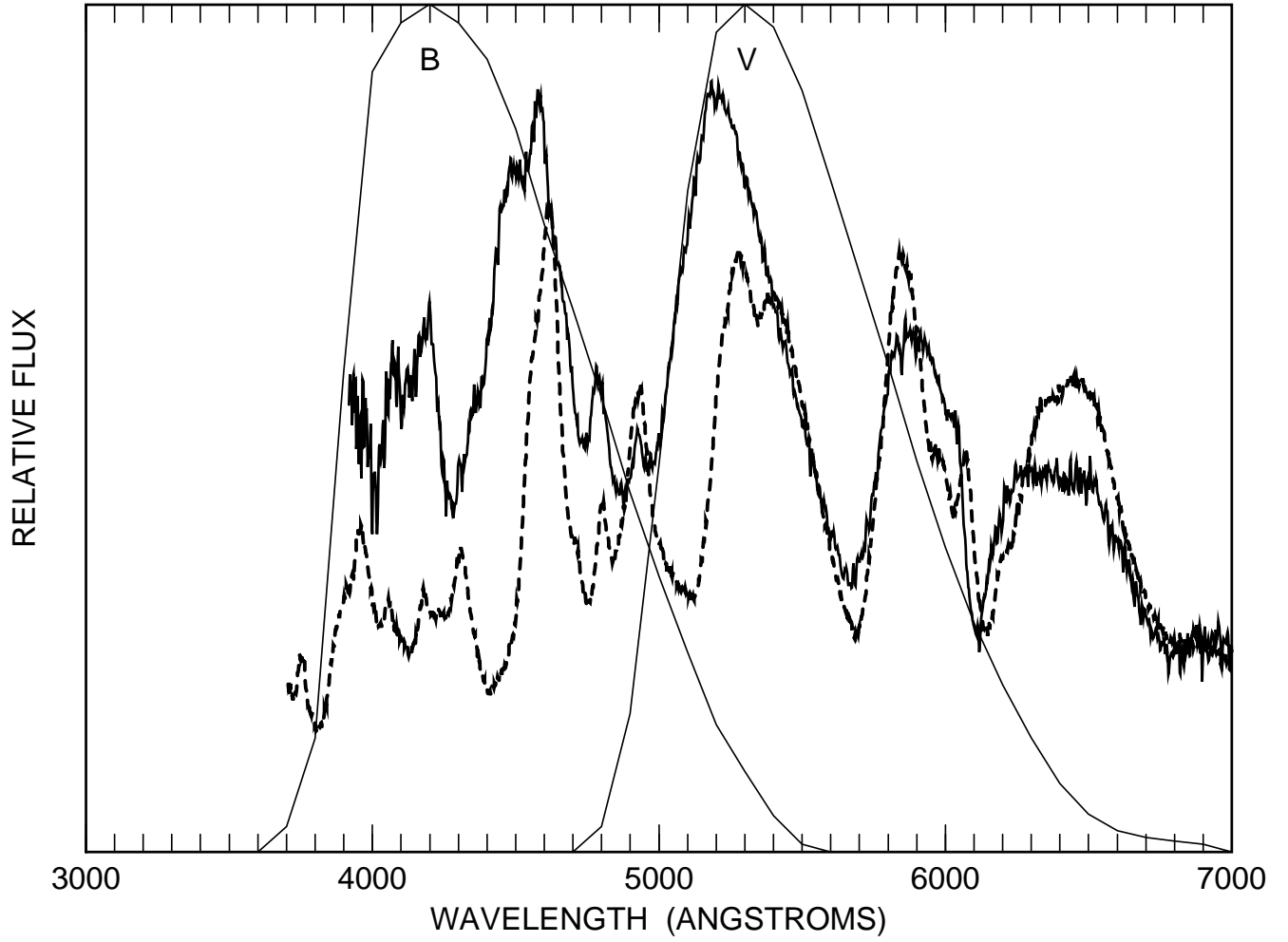


Fig. 12.— The day 15 spectrum of SN 2000cx (*thick solid line*) is compared with a day 18 spectrum of the normal SN Ia 1998aq (*dashed line*). The *B*-band and *V*-band filter functions are also shown (*thin solid lines*).

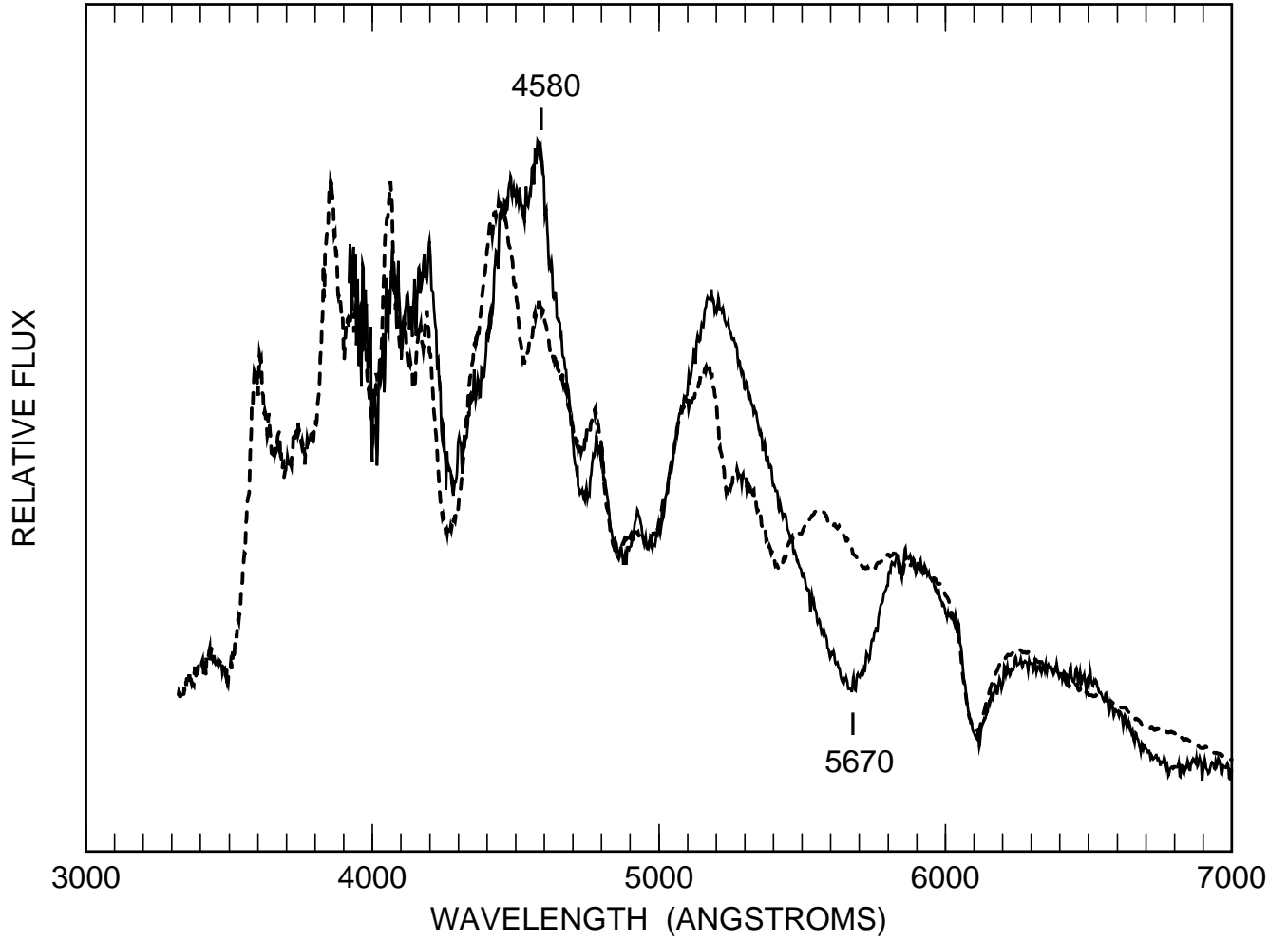


Fig. 13.— The day 15 (*solid line*) and day 7 (*dashed line*) spectra of SN 2000cx are compared.

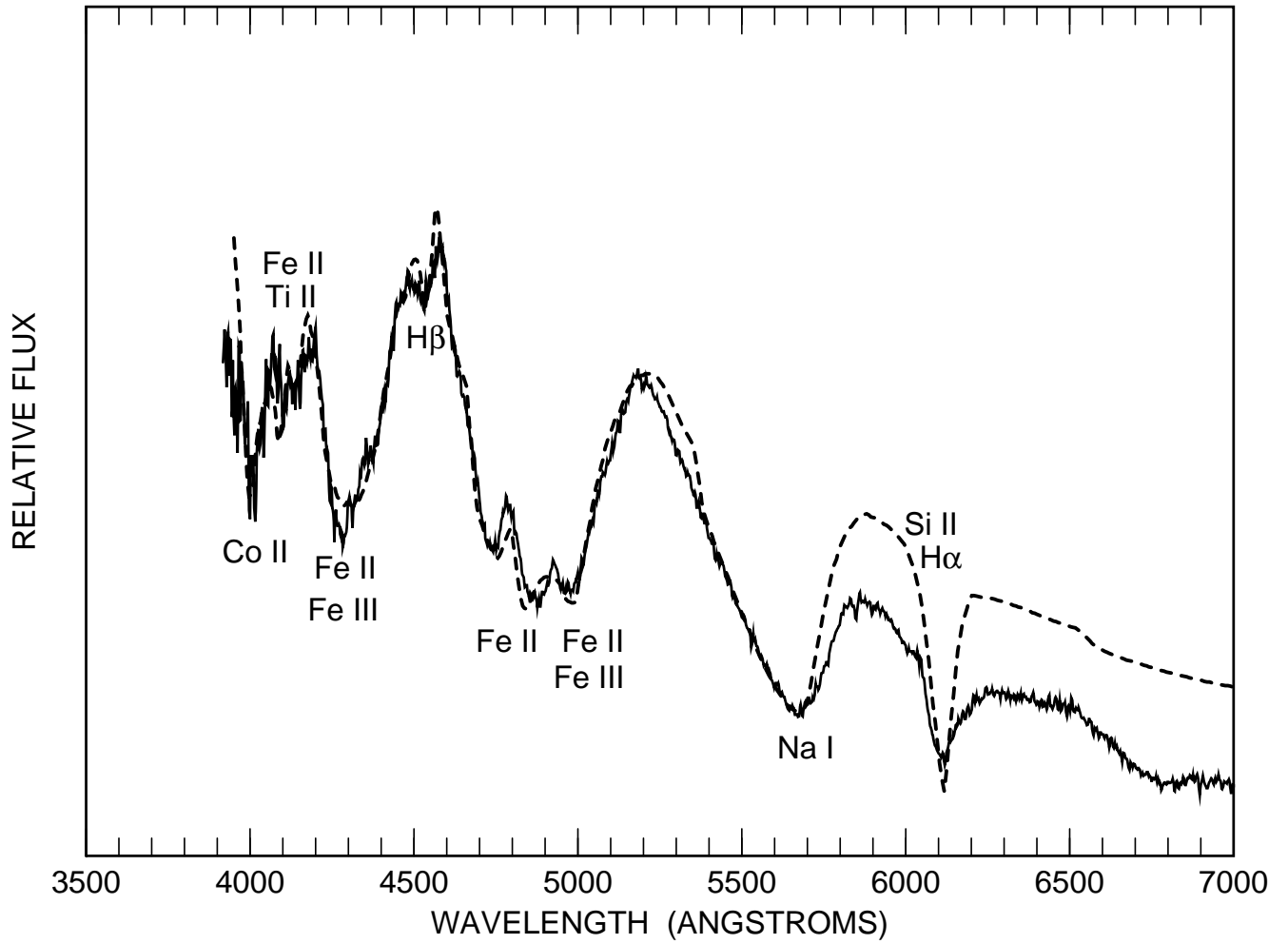


Fig. 14.— The day 15 spectrum of SN 2000cx (*solid line*) is compared with a synthetic spectrum (*dashed line*) that has $v_{phot} = 10,000 \text{ km s}^{-1}$, $T_{bb} = 12000 \text{ K}$, and contains lines of five ions.

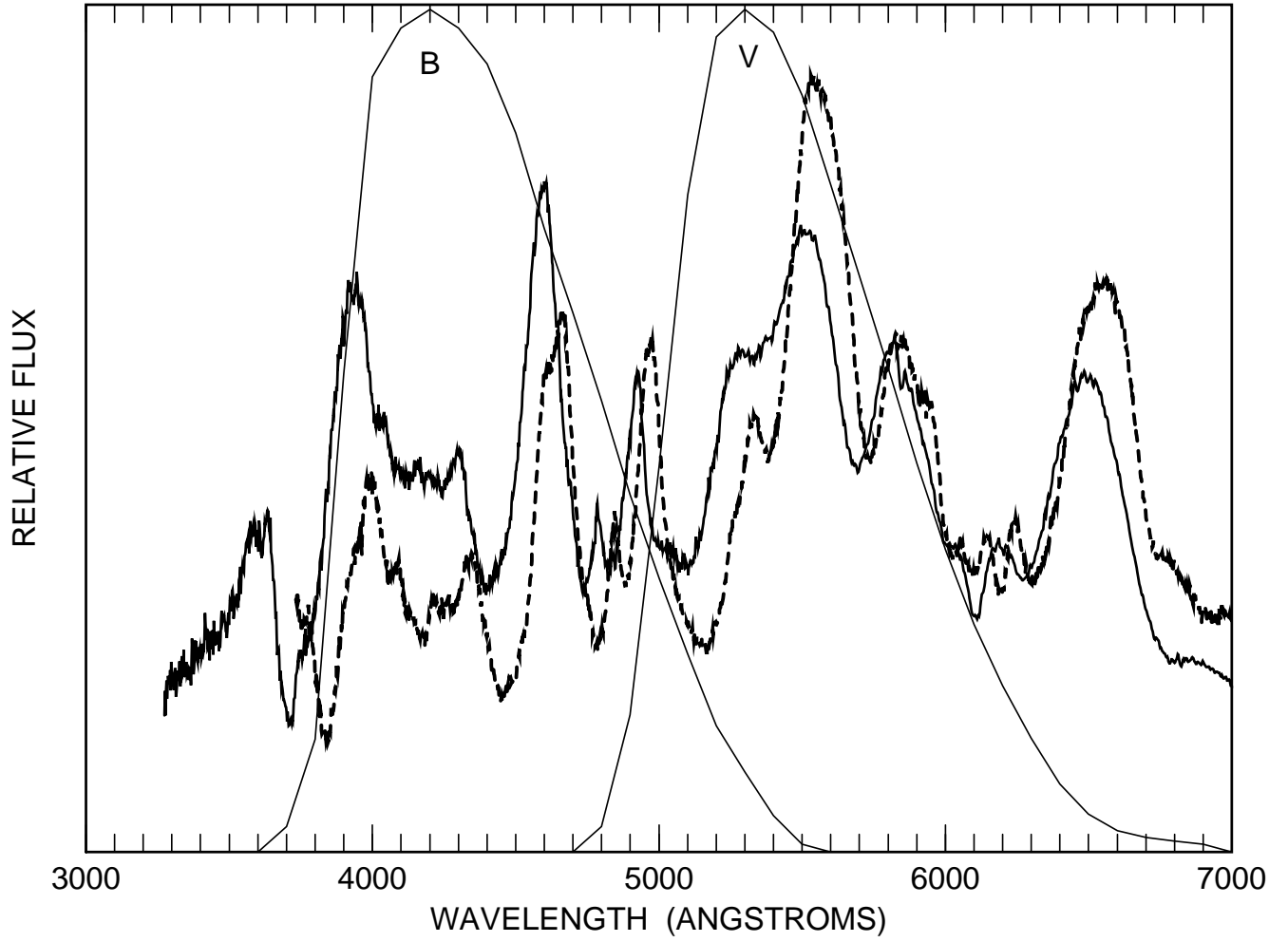


Fig. 15.— The day 32 spectrum of SN 2000cx (*thick solid line*) is compared with a day 32 spectrum of the normal SN Ia 1998aq (*dashed line*). The *B*-band and *V*-band filter functions are also shown (*thin solid lines*).

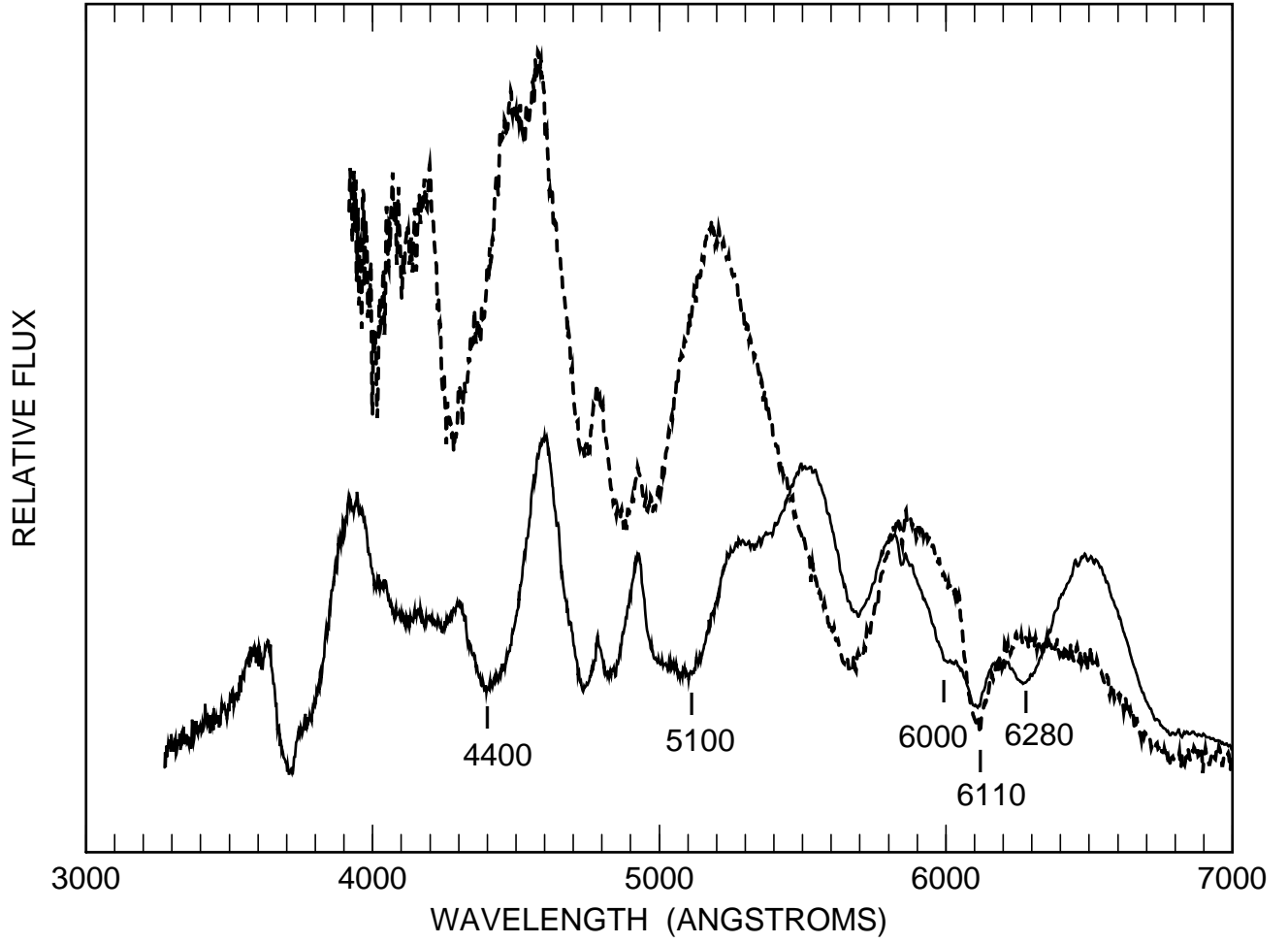


Fig. 16.— The day 32 (*solid line*) and day 15 spectra (*dashed line*) of SN 2000ex are compared.

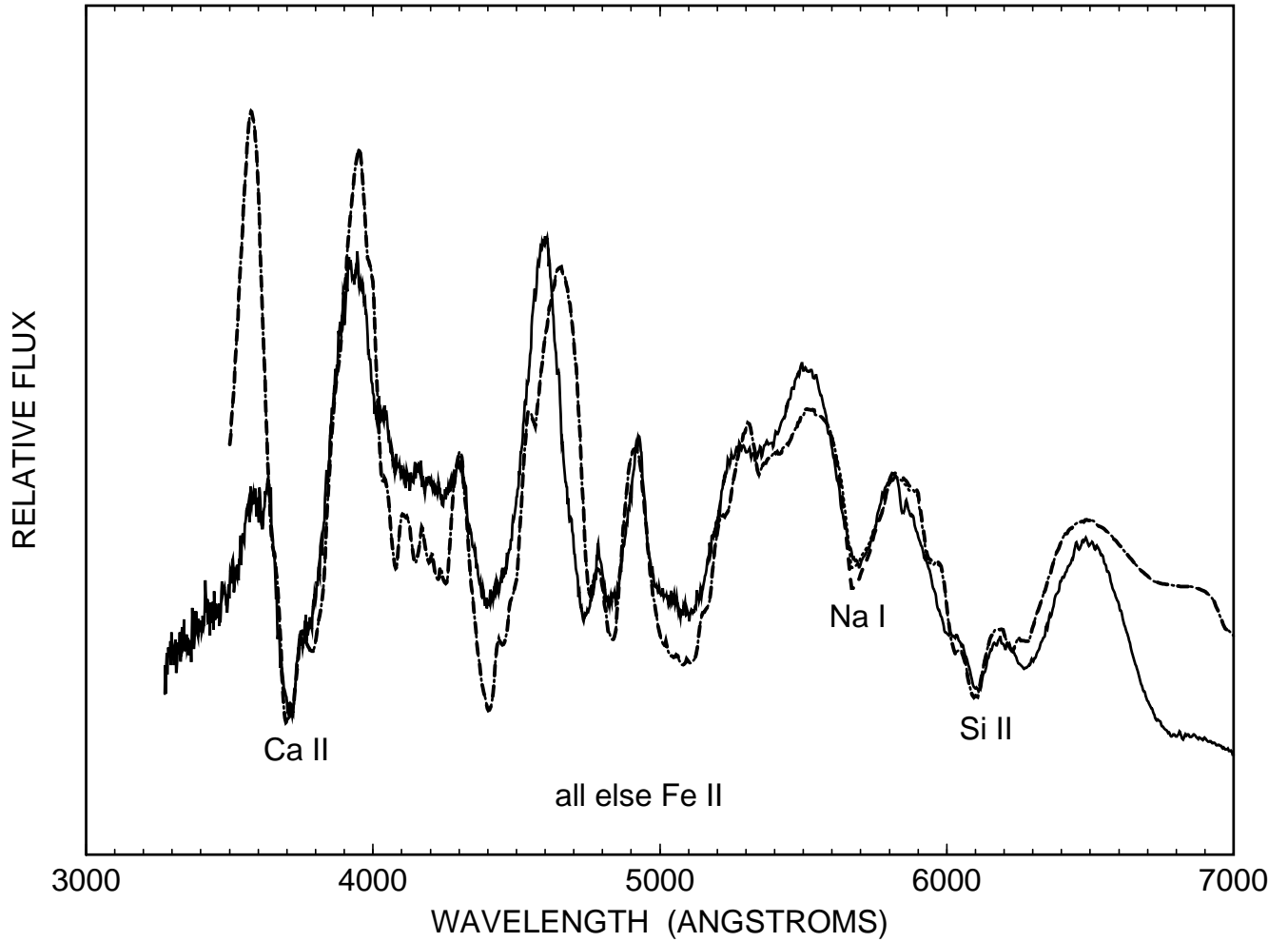


Fig. 17.— The day 32 spectrum of SN 2000cx (*solid line*) is compared with a synthetic spectrum (*dashed line*) that has $v_{phot} = 11,000 \text{ km s}^{-1}$, $T_{bb} = 8000 \text{ K}$, and contains lines of four ions. All unlabelled features in the synthetic spectrum are produced by Fe II.

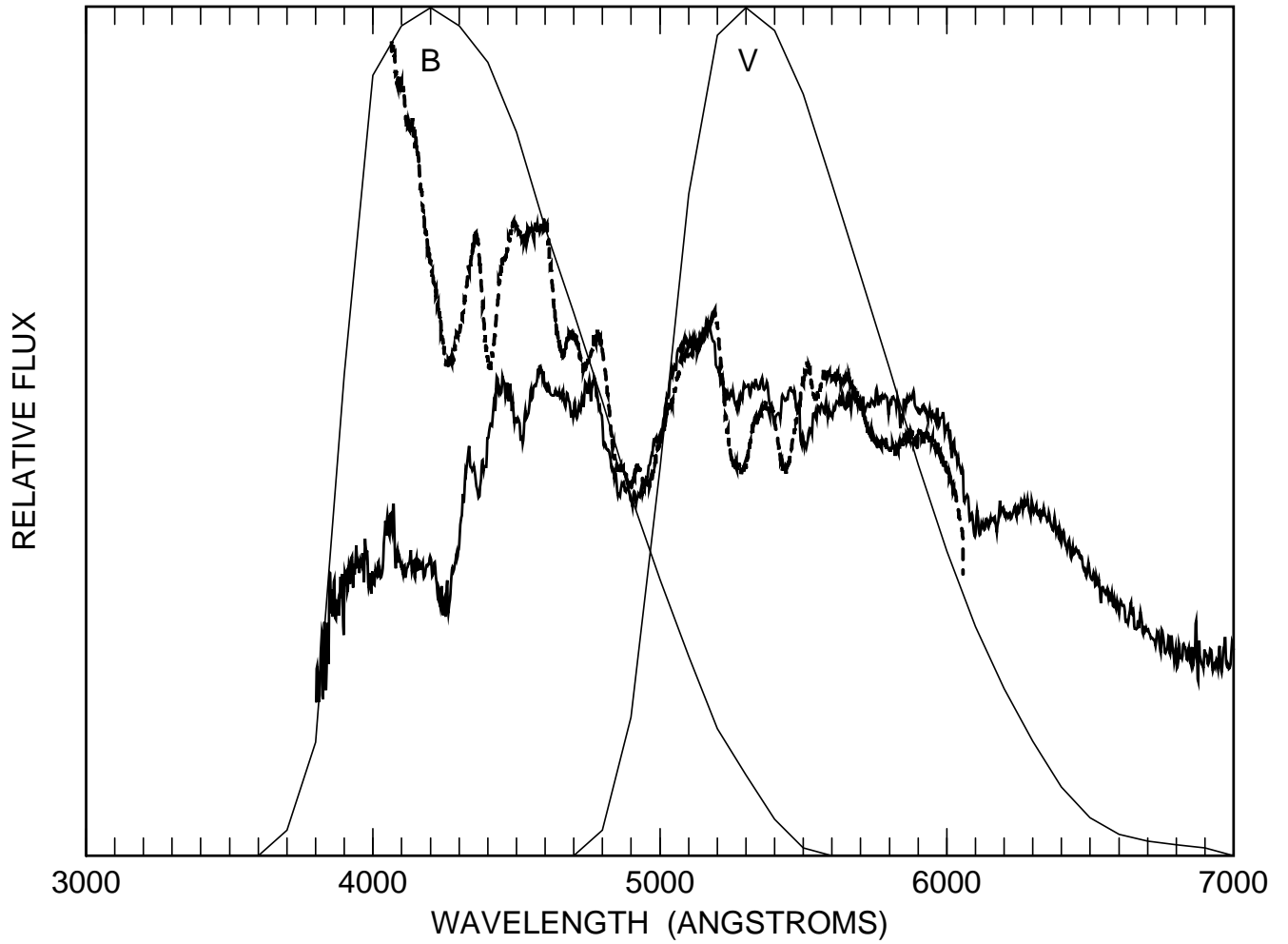


Fig. 18.— The day -3 spectrum of SN 2000cx (*solid line*) is compared with a day -3 spectrum of the normal SN Ia 1998aq (*dashed line*). The B -band and V -band filter functions are also shown (*thin solid lines*).

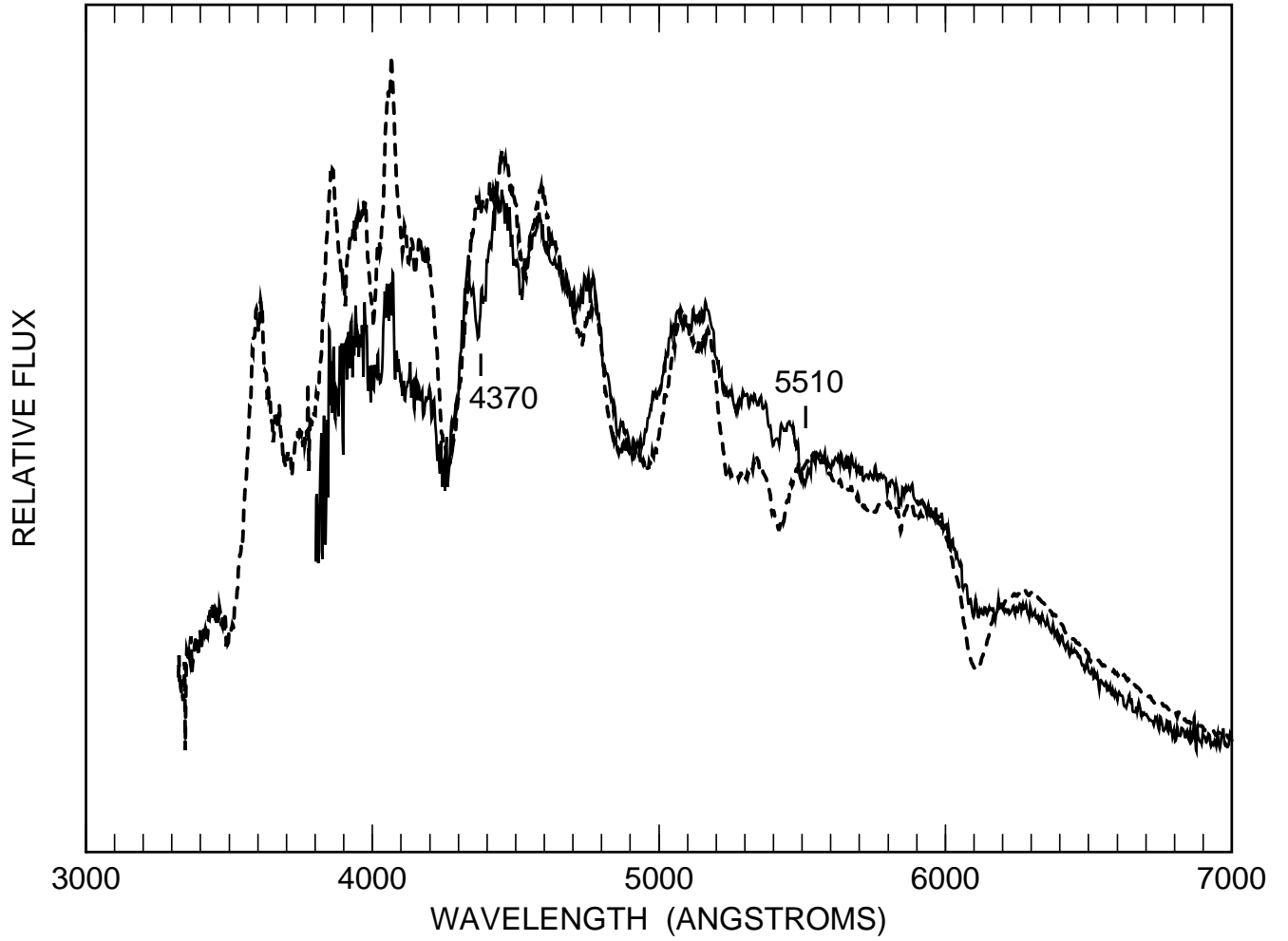


Fig. 19.— The day -03 (*thick solid line*) and day 2 (*dashed line*) spectra of SN 2000cx are compared.

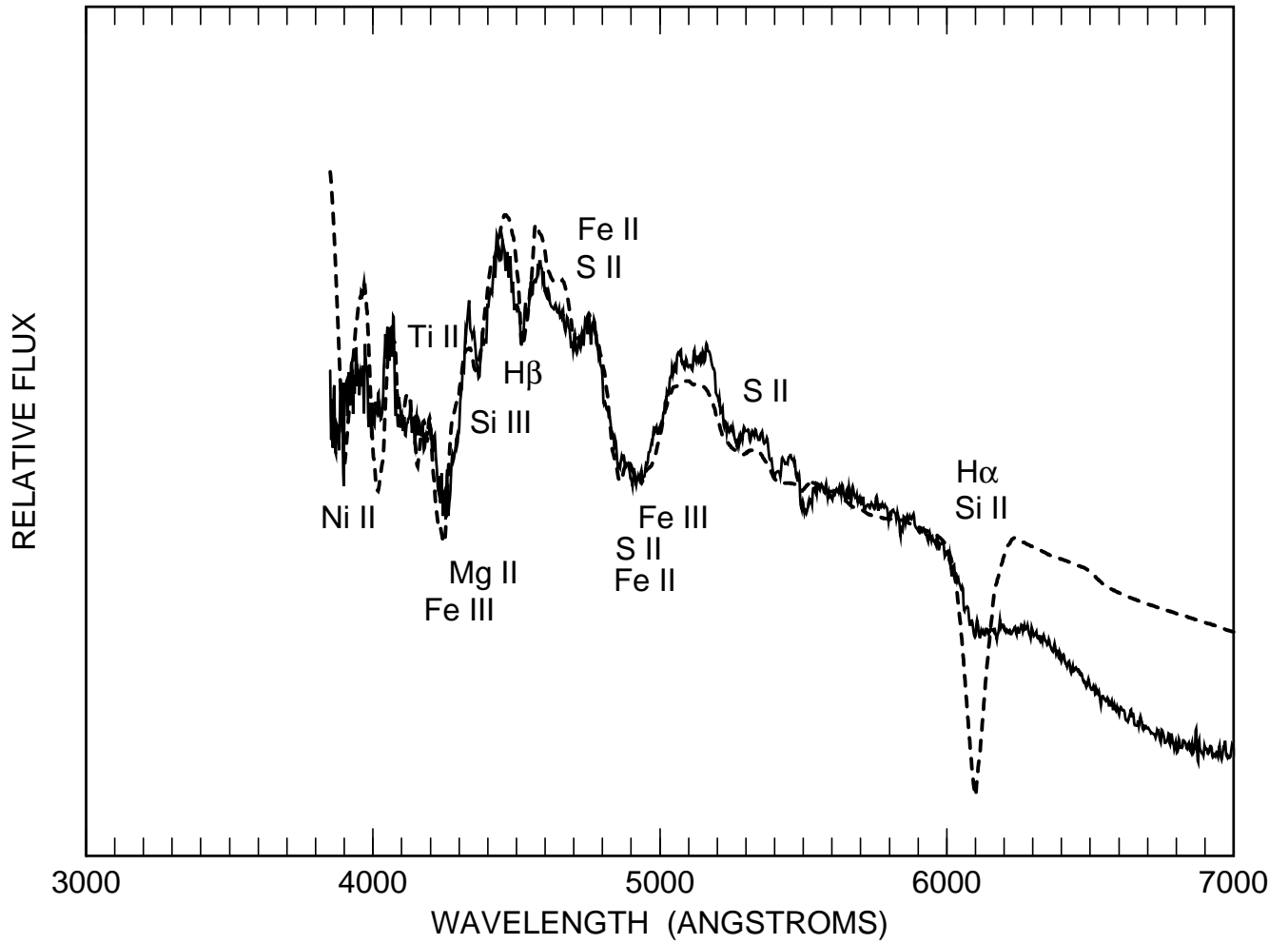


Fig. 20.— The day -3 spectrum of SN 2000cx (*solid line*) is compared with a synthetic spectrum (*dashed line*) that has $v_{phot} = 12,000 \text{ km s}^{-1}$, $T_{bb} = 9000 \text{ K}$, and contains lines of nine ions.

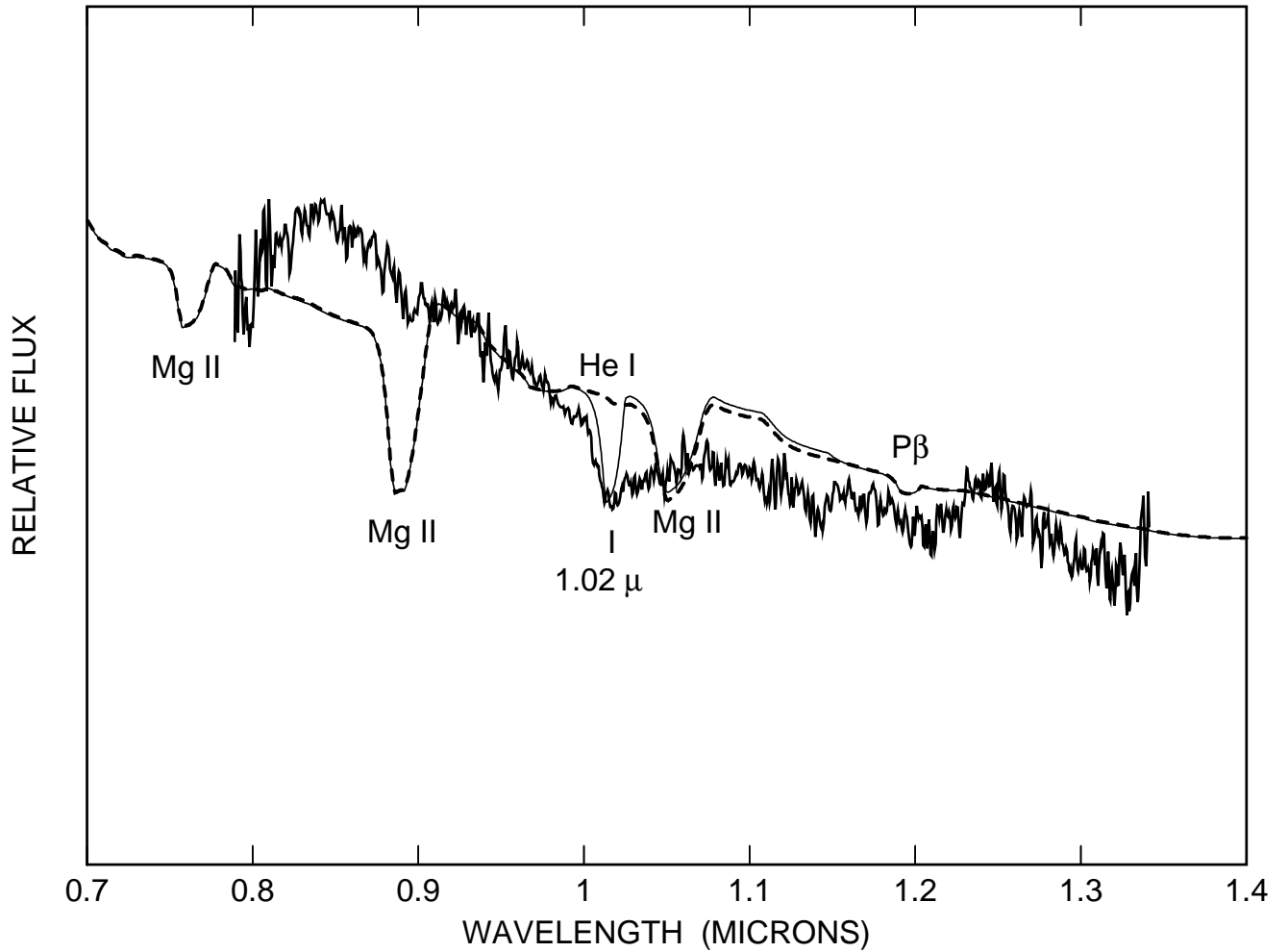


Fig. 21.— The day -5.5 short-wavelength infrared spectrum of SN 2000cx (*solid line*) is compared with an extension of the synthetic spectrum (*dashed line*) of Figure 15 for the day -3 optical spectrum, and the same synthetic spectrum but with the inclusion of He I lines detached at $22,000 \text{ km s}^{-1}$ (*thin solid line*).

Table 1. Input Parameters for Figure 4 (Day 2)

ion	$\lambda(\text{ref})$ (Å)	$\tau(\text{ref})$	v_{min} (km s ⁻¹)	v_{max} (km s ⁻¹)	v_e (km s ⁻¹)	T_{exc} (K)
Mg II	λ4481	1.8	13000	∞	1000	7000
Si II	λ6347	1.5	13000	∞	1000	7000
S II	λ5454	1.3	13000	∞	1000	10000
Ca II	λ3934	2.0	11000	23000	8000	5000
Ca II	λ3934	0.7	23000	∞	3000	5000
Ti II	λ4550	0.4	23000	∞	1000	5000
Fe II	λ5018	0.25	21000	∞	1000	5000
Fe III	λ5156	2.0	13000	∞	1000	14000
Co II	λ4161	1.5	13000	∞	1000	7000
Ni II	λ4067	3.0	13000	∞	1000	7000

Table 2. Input Parameters for Figure 11 (Day 7)

ion	$\lambda(\text{ref})$ (\AA)	$\tau(\text{ref})$	v_{min} (km s^{-1})	v_{max} (km s^{-1})	v_e (km s^{-1})	T_{exc} (K)
H I	$\lambda 6563$	7.0	22000	∞	1000	5000
Mg II	$\lambda 4481$	2.5	13000	∞	1000	7000
Si II	$\lambda 6347$	1.0	13000	∞	1000	8000
S II	$\lambda 5454$	1.0	13000	∞	1000	10000
Ca II	$\lambda 3934$	2.5	11000	23000	8000	5000
Ca II	$\lambda 3934$	0.8	23000	∞	3000	5000
Ti II	$\lambda 4550$	0.6	23000	∞	1000	5000
Fe II	$\lambda 5018$	0.6	19000	∞	2000	7000
Fe III	$\lambda 5156$	2.5	13000	∞	1000	14000
Co II	$\lambda 4161$	2.0	13000	∞	1000	7000
Ni II	$\lambda 4067$	4.0	13000	∞	1000	7000

Table 3. Input Parameters for Figure 14 (Day 15)

ion	$\lambda(\text{ref})$ (Å)	$\tau(\text{ref})$	v_{min} (km s ⁻¹)	v_{max} (km s ⁻¹)	v_e (km s ⁻¹)	T_{exc} (K)
H I	λ6563	4.0	22000	∞	1000	5000
Na I	λ5892	1.5	10000	∞	7000	5000
Si II	λ6347	2.0	13000	∞	1000	7000
Ti II	λ4550	0.3	23000	∞	1000	5000
Fe II	λ5018	0.7	11000	23000	20000	7000
Fe III	λ5156	2.5	10000	∞	1000	14000
Co II	λ4161	1.0	13000	∞	1000	7000

Table 4. Input Parameters for Figure 17 (Day 32)

ion	$\lambda(\text{ref})$ (\AA)	$\tau(\text{ref})$	v_{min} (km s^{-1})	v_{max} (km s^{-1})	v_e (km s^{-1})	T_{exc} (K)
Na I	$\lambda 5892$	1.5	12000	∞	1000	5000
Si II	$\lambda 6347$	2.0	13000	∞	1000	7000
Ca II	$\lambda 3934$	4.0	11000	20000	3000	5000
Ca II	$\lambda 3934$	2.0	20000	∞	1000	5000
Fe II	$\lambda 5018$	100	11000	13000	2000	10000
Fe II	$\lambda 5018$	2.0	13000	∞	1000	7000

Table 5. Input Parameters for Figure 20 (Day –3)

ion	$\lambda(\text{ref})$ (\AA)	$\tau(\text{ref})$	v_{min} (km s^{-1})	v_{max} (km s^{-1})	v_e (km s^{-1})	T_{exc} (K)
H I	$\lambda 6563$	7.0	23000	∞	1000	5000
Mg II	$\lambda 4481$	1.0	13000	∞	1000	7000
Si II	$\lambda 6347$	0.2	14000	∞	1000	7000
Si III	$\lambda 4550$	1.5	14000	∞	1000	14000
S II	$\lambda 5454$	0.2	14000	∞	1000	10000
Ti II	$\lambda 4550$	0.7	23000	∞	1000	5000
Fe II	$\lambda 5018$	0.5	21000	∞	1000	7000
Fe III	$\lambda 5156$	1.0	14000	∞	1000	14000
Ni II	$\lambda 4067$	1.0	13000	∞	1000	7000